

# CAUSALKANS: INTERPRETABLE TREATMENT EFFECT ESTIMATION WITH KOLMOGOROV-ARNOLD NETWORKS

Alejandro Almodóvar\* Patricia A. Apellániz Santiago Zazo Juan Parras

Information Processing and Telecommunications Center, ETSI de Telecomunicación  
Universidad Politécnica de Madrid  
Madrid, Spain

## ABSTRACT

Deep neural networks achieve state-of-the-art performance in estimating heterogeneous treatment effects, but their opacity limits trust and adoption in sensitive domains such as medicine, economics and public policy. Building on well-established and high-performing causal neural architectures, we propose *causalKANs*, a framework that transforms neural estimators of *conditional average treatment effects* (CATEs) into Kolmogorov–Arnold Networks (KANs). By incorporating pruning and symbolic simplification, causalKANs yields interpretable closed-form formulas while preserving predictive accuracy. Experiments on benchmark datasets demonstrate that causalKANs perform on par with neural baselines in CATE error metrics, and that even simple KAN variants achieve competitive performance, offering a favorable accuracy–interpretability trade-off. By combining reliability with analytic accessibility, causalKANs provide auditable estimators supported by closed-form expressions and interpretable plots, enabling trustworthy individualized decision-making in high-stakes settings. We release the code for reproducibility in <https://github.com/aalmodovares/causalkans>.

## 1 INTRODUCTION

Estimating individual treatment effects from observational data underpins high-stakes decisions in personalized medicine (Kent et al., 2018; Sanchez et al., 2022), public policy (Imai and Strauss, 2011), and economics (Manski, 2004), where interventions must be tailored beyond population averages (Wager and Athey, 2018). As personalized decision-making becomes the norm, accurately recovering conditional average treatment effects (CATEs) is indispensable for policy targeting and individualized care (Curth et al., 2024). However, accuracy alone is insufficient: regulatory frameworks (GDPR Art. 22; EU AI Act transparency for high-risk AI) and clinical practice increasingly discourage opaque models in consequential settings (European Parliament and Council, 2016; 2024; Goodman and Flaxman, 2017). Indeed, limited interpretability remains a barrier to the clinical adoption of machine learning (ML) systems (Amann et al., 2020; Tonekaboni et al., 2019). Yet contemporary state-of-the-art CATE estimators often rely on deep neural networks (Shalit et al., 2017; Shi et al., 2019), which we call *causalNN*, achieving strong performance but hindering auditing and trustable deployment.

We address this gap proposing *causalKANs*: a practical framework that transforms, or *KAN-ifies* (see Fig. 1), neural CATE estimators into *closed-form*, auditable models by replacing their sub-networks with Kolmogorov–Arnold Networks (KANs) (Liu et al., 2024a;b). KANs parameterize one-dimensional edge functions (splines) and compose them via sums (and, in variants, products), enabling post-training simplification without departing from the trained predictor. Our interpretability notion is operational: after training, we apply edge-activity regularization, validation-guided

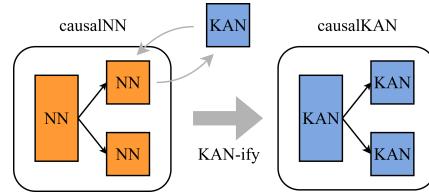


Figure 1: KAN-ification.

\*correspondence author [alejandro.almodovar@upm.es](mailto:alejandro.almodovar@upm.es)

pruning, and auto-symbolic substitution of learned splines with simple atoms to produce executable expressions for the potential outcomes and their difference (the CATE).

Concretely, our **contributions** are twofold. First, we introduce a **model-agnostic framework** for constructing KAN-based potential-outcome models from established causal neural architectures (e.g., metalearners (Künzel et al., 2019), TARNet (Shalit et al., 2017), DragonNet (Shi et al., 2019)) while reusing their training objectives (see Fig. 1 for a sketch). Second, we present an **empirical study** on two well known benchmark datasets (IHDP (Hill, 2011) and ACIC (Dorie et al., 2017)), demonstrating that at least one causalKAN variant matches or surpasses neural baselines in causal metrics while delivering closed-form CATEs, as can be seen in Fig. 2, where, although there are difference between causalKANs and their respective MLP-counterparts, one causalKAN is among the best models. Code and scripts are released for full reproducibility in <https://github.com/aalmodovares/causalkans>.

Our study positions causalKANs as domain-agnostic, accuracy-preserving, and inspection-ready CATE estimators: they retain the flexibility of deep architectures yet yield executable formulas that make effect modifiers and interactions explicit, aligning with emerging requirements for trustworthy, human-auditable decision support.

Empirically, causalKANs provide a favorable accuracy–interpretability frontier: simple heads (often additive or one hidden KAN layer) achieve competitive metrics across benchmarks, while additional depth rarely improves accuracy and consistently reduces formula compactness. We present the preliminaries in §3, the causalKANs pipeline and instantiations in §4, and reports ablations, comparisons, and interpretability results in §5.

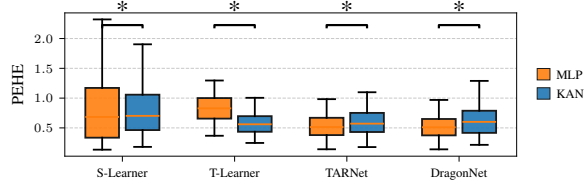


Figure 2: Overall, causalKANs achieves similar PEHE (lower is better) than causalNNs in IHDP A. \* means statistical difference  $p < 0.05$  in a Wilcoxon paired test.

## 2 RELATED WORK

Kolmogorov-Arnold networks, as interpretable and parameter efficient alternatives of multi-layer perceptrons (MLP), have experienced a great growth in the last year, with the adaptation of existing technologies as convolutional networks (Bodner et al., 2024), residual networks (Yu et al., 2024), quantum networks (Wakaura et al., 2025), or autoencoders (Moradi et al., 2024). In the same manner, they have had an impressive adoption in domains where transparency is critical, as predicting risks in cardiovascular diseases (Al Bataineh et al., 2025) in healthcare (Almodóvar et al., 2025; Pendyala and Venkatachalam, 2025); predicting volatility in finances (Cho et al., 2025); predicting biomarkers (Alharbi et al., 2025), or predicting physics in power systems (Shuai and Li, 2025).

Interpretability is widely regarded as essential for the adoption of ML in sensitive domains (Doshi-Velez and Kim, 2017). Methods for improving interpretability based on KANs have been used in critical domains, such as Kolmogorov-Arnold Additive Models (KAAMs) (Almodóvar et al., 2025), which are shallow KANs that yields nonlinear additive models, which are well known as interpretable flexible estimators, as Neural Additive Models (NAMs) (Agarwal et al., 2021) or generalized additive models (Caruana et al., 2015). A closely related line is *symbolic regression* (SR), which searches over expression trees to recover closed-form models, classically via genetic programming (Schmidt and Lipson, 2009) and can produce highly concise formulas; however, SR is also computationally intensive and scales poorly (Zhang et al., 2022), while KANs, optimized by gradient descent, have been reported to be parameter-efficient and fast to optimize in practice (Liu et al., 2024b).

The need for interpretability is equally pressing in causal inference, where estimators are expected not only to predict counterfactuals but also to justify treatment decisions (Athey and Imbens, 2016). Early approaches such as causal trees (Athey and Imbens, 2016) provided transparent rule sets, and linear regressors were interpretable through their coefficients as causal parameters (Hahn et al., 2018). However, partially interpretable algorithms like causal forests (Foster et al., 2011) and BART (Hill, 2011) offered better predictive accuracy, while neural networks advanced performance even further (Johansson et al., 2016; Schwab et al., 2018; Shalit et al., 2017; Yao et al., 2018; Yoon et al., 2018) at

the cost of opacity. As a result, interpretability has often been relegated to a secondary concern in causal estimation (Rudin, 2018).

Bridging the trade-off between accuracy and transparency remains challenging. Some promising attempts include NAM-based estimators of average treatment effects (Chen et al., 2025), attention-based transformers highlighting confounder importance (Zhang et al., 2023), causal rule learners that yield decision rules but rely on black-box induction (Bargagli-Stoffi et al., 2024; Wu et al., 2025), and fused lasso regression-based methods producing interpretable effect curves (Padilla et al., 2025). *Model distillation* approaches, such as training a surrogate on top of the work of Shalit et al. (2017) (Kim and Bastani, 2021), offer another path but depend on surrogate fidelity. Yet, addressing causal inference and interpretability together requires further work (Moraffah et al., 2020). In this context, KAN-inspired models such as our approach are promising because they combine the interpretability of additive structures with an expressive power undistinguishable of that of neural networks.

To the best of our knowledge, we are the second work that employs KANs for causal estimation, after KANITE (Mehendale et al., 2025), which replaces MLP backbones with KANs to estimate individual treatment effects under multiple treatments, using integral probability metrics/entropy-balancing variants and reporting gains in causal inference metrics over strong baselines. Its emphasis is predictive accuracy; it neither targets interpretability nor provides closed-form effect functions or visually interpretable plots. Instead, our work focuses on extracting human-readable causal effect formulas.

### 3 PRELIMINARIES

We consider an observational dataset  $\mathcal{D} = \{\mathbf{x}_i, t_i, y_i\}_{i=1}^N$  of  $N$  i.i.d. samples from an unknown distribution  $P(\mathbf{x}, \mathbf{t}, \mathbf{y})$ , where  $\mathbf{x} \in \mathcal{X} \subset \mathbb{R}^D$  are covariates,  $\mathbf{t} \in \mathcal{T} = \{0, 1\}^1$  is the treatment, and  $\mathbf{y} \in \mathbb{R}$  is the outcome. Our goal is to estimate the causal effect of the treatment on the outcome and provide a closed-form, interpretable formula for it.

Following the Neyman–Rubin potential outcomes framework (Rubin, 1974; Splawa-Neyman et al., 1990), each individual  $i$  has potential outcomes  $\mathbf{y}_i(t)$  for  $t \in \{0, 1\}$ . Only the outcome corresponding to the received treatment is observed, which constitutes the *fundamental problem of causal inference*. The target estimand is the individual treatment effect (ITE):  $\tau_i = \mathbf{y}_i(1) - \mathbf{y}_i(0)$ .

Since  $\tau_i$  is not observable, we estimate instead the conditional average treatment effect (CATE):

$$\tau(\mathbf{x}) := \mathbb{E}[\mathbf{y}(1) \mid \mathbf{x} = \mathbf{x}] - \mathbb{E}[\mathbf{y}(0) \mid \mathbf{x} = \mathbf{x}], \quad \text{denoting} \quad \mu_t(\mathbf{x}) := \mathbb{E}[\mathbf{y}(\mathbf{t}) \mid \mathbf{x} = \mathbf{x}]. \quad (1)$$

We assume the standard conditions of causal inference: **i) positivity**,  $0 < P(\mathbf{t} = t \mid \mathbf{x}) < 1$ ; **ii) conditional ignorability**,  $\mathbf{y}(t) \perp\!\!\!\perp \mathbf{t} \mid \mathbf{x}$ , which requires a valid adjustment set blocking all backdoor paths<sup>2</sup>; **iii) consistency**,  $\mathbf{y}_i(t_i) = y_i$ ; and **iv) no interference**,  $\mathbf{y}_i \perp\!\!\!\perp \mathbf{y}_j$  for  $i \neq j$ . Under these assumptions, it follows that  $\mathbb{E}[\mathbf{y} \mid \mathbf{x}, \mathbf{t}]$  is an unbiased estimator of  $\mu_t(\mathbf{x})$  (Hernán and Robins, 2025). The challenge is that this conditional expectation becomes increasingly difficult to estimate with high-dimensional, multimodal covariates and complex covariate–treatment–outcome relations, motivating the use of flexible function approximators such as neural networks.

#### 3.1 CAUSAL NEURAL NETWORKS

Neural networks are flexible function approximators (Hornik et al., 1989) and often provide state-of-the-art potential–outcome and CATE estimates (Alaa and Schaar, 2018; Curth and Van der Schaar, 2021b; Tesei et al., 2023). We summarize the canonical architectures used in our experiments (see Fig. 3); all perform potential–outcome regression,  $\mu_t(\mathbf{x})$ , and obtain the CATE by difference,  $\hat{\tau}(\mathbf{x}) = \hat{\mu}_1(\mathbf{x}) - \hat{\mu}_0(\mathbf{x})$ . Our replacement of neural backbones by KANs is orthogonal to these designs and can also be applied to methods that target CATE directly (e.g., X-, R-learners, MRIV-Net; Frauen and Feuerriegel, 2022; Künzel et al., 2019; Nie and Wager, 2021).

<sup>1</sup>We focus on binary treatments for clarity, though the derivations extend to multi-valued and in some cases continuous treatments; see §A.1.

<sup>2</sup>An adjustment set must block all backdoor paths between treatment and outcome, avoid selection bias, and not block front-door paths.

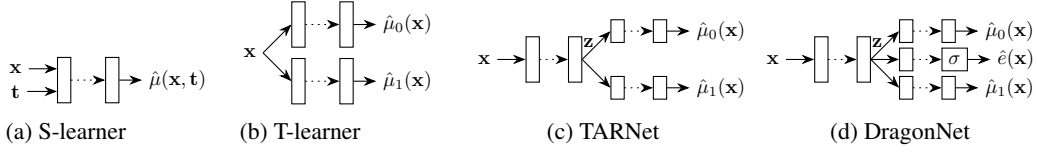


Figure 3: Architectures used for *potential outcome regression*. Boxes denote layers or backbones (neural networks or KANs); dotted arrows indicate optional hidden layers.

**Meta-learners** (Künzel et al., 2019) are model-agnostic. The *S-learner* fits a single regressor  $\mu_t(\mathbf{x}, t)$  of the factual outcome and obtains potential outcomes by toggling  $t$ . Its simplicity and ability to handle continuous treatments are appealing, but it may underuse  $t$  when the treatment signal is weak relative to  $\mathbf{x}$ . The *T-learner* trains two separate regressors,  $\hat{\mu}_0(\mathbf{x})$  and  $\hat{\mu}_1(\mathbf{x})$ , one per arm. This allows treatment-specific fits but splits the data, which can increase variance and yield sharp CATE estimates in small samples.

**TARNet** (Shalit et al., 2017) introduces a shared representation  $\mathbf{z}(\mathbf{x})$  feeding two heads, combining the strengths above: shared structure across arms (mitigating data inefficiency) with treatment-specific outcome mappings (reducing treatment ignorance). Its CFRNet variant changes only the loss to encourage balanced representations, while the architecture remains identical. TARNet has shown robust performance and is widely used as a baseline (Curth and Van der Schaar, 2021a;b; Schwab et al., 2018; Shalit et al., 2017; Yao et al., 2018).

**DragonNet** (Shi et al., 2019) extends TARNet with a third head for the propensity score,  $\hat{e}(\mathbf{x})$ , encouraging  $\mathbf{z}(\mathbf{x})$  to capture confounding structure through multitask learning. Originally paired with targeted regularization for doubly robust average treatment effect (ATE) estimation (Van der Laan et al., 2011), the base network already yields accurate potential outcomes and thus CATEs (Curth and Van der Schaar, 2021b; Ling et al., 2023; Lolak et al., 2025). Intuitively, predicting both outcomes and treatment forces the representation to retain covariates that co-determine assignment and response, which benefits counterfactual prediction.

Fig. 3 illustrates the corresponding schematics; we keep the architectures unchanged when replacing neural components by KANs.

### 3.2 KOLMOGOROV–ARNOLD NETWORKS

We employ KANs as our backbones. Kolmogorov–Arnold Networks (KANs) (Liu et al., 2024b) are deep models that replace fixed node-wise activations with *learnable univariate functions on edges*, using *addition*—and, in extensions, multiplication (Liu et al., 2024a)—as the only explicit multivariate operations. Their design is motivated by the Kolmogorov–Arnold representation theorem (KART), which guarantees that any continuous  $f : \mathbb{R}^D \rightarrow \mathbb{R}$  can be expressed as

$$f(\mathbf{x}) = \sum_{q=1}^{2D+1} \Phi_q \left( \sum_{k=1}^D \phi_{q,k}(x_k) \right), \quad (2)$$

where all nonlinearities are one-dimensional (Arnold, 1957; Braun and Griebel, 2009; Kolmogorov, 1956; 1957). This motivates stacked architectures where multivariate structure emerges from compositions of simple univariate transformations and aggregations. Formally, a depth- $L$  KAN with widths  $\{n_l\}$  and coordinates  $z_{l,r}$  replaces the linear map and fixed activation at layer  $l$  by

$$z_{l+1,s} = \sum_{r=1}^{n_l} \phi_{l,s,r}(z_{l,r}), \quad s = 1, \dots, n_{l+1}, \quad (3)$$

so that the whole network computes:  $\text{KAN}(\mathbf{x}) = (\Phi_{L-1} \circ \Phi_{L-2} \circ \dots \circ \Phi_0)(\mathbf{x})$ . Each  $\phi_{l,s,r}$  is parameterized as a smooth B-spline,

$$\phi(z) = w_b b(z) + w_s \text{spline}(z),$$

with  $b(z)$  a fixed baseline (e.g., identity or SiLU), and  $w_s, w_b$  are learnable weights. This construction is fully differentiable and trainable with standard backpropagation. While the shallow KART decom-

position may involve irregular univariates, stacking layers yields smooth, accurate approximations (Liu et al., 2024b).

KANs retain universal approximation: refining spline grids (internal degrees of freedom) and stacking layers (external degrees of freedom) expands expressivity while exposing interpretable one-dimensional components. Compared to MLPs with fixed nonlinearities, complexity shifts from dense weight matrices to a small number of spline coefficients per edge, making the active graph (which edges matter) separable from the functional form of each transformation. Training follows standard optimizers and losses, with sparsity encouraged by  $\ell_1$  or group penalties that prune low-contribution edges. The pruned networks are compact, with remaining splines straightforward to inspect or approximate symbolically. The *MultKAN* extension (Liu et al., 2024a) further augments summation nodes with parameter-free multiplication nodes, explicitly representing interactions without forcing splines to emulate them.

In summary, KANs are deep models built from learnable one-dimensional splines composed through sums (and optionally products). They preserve universal approximation, train with off-the-shelf methods, admit effective pruning, and expose interpretable building blocks at the level of univariate functions and explicit interactions. These properties make them natural candidates to replace neural backbones in causalKANs.

## 4 CAUSAL KOLMOGOROV–ARNOLD NETWORKS

We introduce *causalKANs*, a framework that replaces the neural components of standard potential–outcome regressors with Kolmogorov–Arnold Networks (KANs), and augments training with *pruning* and *auto-symbolic search* to yield analytic, interpretable CATE formulas. The approach is model-agnostic: any causalNN can be converted by swapping MLP blocks with KAN (or MultKAN) blocks while keeping inputs and outputs unchanged, and using the same loss functions as their neural counterparts but augmented with regularization terms.

### 4.1 INTERPRETABLE CAUSAL LEARNING

Our goal is to deliver *closed-form* and *auditable* estimates of  $\hat{\tau}(x) = \hat{\mu}_1(x) - \hat{\mu}_0(x)$  without sacrificing the flexibility of deep learning. To this end, we expose a pipeline in which the practitioner controls each simplification step, chooses which steps to perform, and sets explicit performance budgets that cap the error introduced by simplification. The five stages are shown in Fig. 17; architecture substitution is illustrated in Fig. 1, and implementation details are in §B.

1. **KAN-ification (architecture swap).** Choose a causalNN (e.g., S-KAN, T-KAN, TARKAN, DragonKAN) and replace each MLP subnetwork by a KAN block with matching input/output dimensions. When the original network has multiple subnetworks, intermediate widths and representation sizes need not be preserved; KAN widths can be reduced to encourage parsimony. MultKAN nodes are optional and only used when explicit interactions are needed (§3.2).
2. **Hyperparameter selection & training.** Tune depth, width, spline grid size, and regularization. During training we employ: **i)** *edge activity* penalty ( $\ell_1$ )  $\lambda_1 \sum_{l,s,r} \mathbb{E} |\phi_{l,s,r}(z_{l,r})|$  to promote sparse parent sets; **ii)** *spline coefficient* regularization  $\lambda_c \sum |w_s| + \lambda_s \sum |w_s - w'_s|$  to shrink magnitudes and encourage smoothness; and **iii)** an *entropy* penalty on fan-in/fan-out to discourage diffuse connectivity. These terms stabilize pruning and symbolification. Early stopping is applied on a validation split. For notational brevity, all penalties are aggregated into  $\mathcal{R}$  in later formulas. Among models with statistically indistinguishable validation metrics, we select the simplest (fewer layers, coarser grids, fewer nodes, no multiplication nodes), which is supported by an ablation study in §C.1. We also compare the predictive loss (excluding  $\mathcal{R}$ ) to the original causalNN; if the causalKAN loss exceeds the baseline by more than a user budget  $\Lambda_{\text{arch}}$ , we revise the KAN design.
3. **Pruning (structure simplification).** On a held-out set, compute edge importance scores

$$s_{l,s,r} = \mathbb{E} [ |\phi_{l,s,r}(z_{l,r})| ], \quad (4)$$

remove edges (and isolated nodes) with  $s_{l,s,r} < \Gamma$ , and retrain briefly if desired. There are alternative pruning techniques, that remove edges based on other metrics, see (Liu et al., 2024a).



This step is optional: if the held-out loss rises beyond a pruning budget  $\Lambda_{\text{prune}}$ , we revert the change. Pruning exposes smaller parent sets and simplifies the subsequent symbolification.

4. **Auto-symbolic search (function simplification).** For each remaining edge function, fit a simple atom from a dictionary (identity, polynomials, tanh, sin, cos, log, exp, etc.) via

$$\min_{m,a,b,c,d} \frac{1}{|\mathcal{V}|} \sum_{z \in \mathcal{V}} \left( \phi_{l,s,r}(z) - [c f_m(az + b) + d] \right)^2. \quad (5)$$

We introduce an interpretability-first inductive bias: attempt the simplest atoms first (polynomials); if the  $R^2$  exceeds a threshold  $\Gamma_{R^2}$ , accept immediately without testing more complex atoms. Otherwise, continue through the dictionary and accept a substitution only if the validation loss increases by at most  $\Lambda_{\text{symb}}$ . If the increase exceeds the budget, revert. This design makes the loss–simplicity trade-off explicit and user-controllable.

5. **CATE extraction and interpretation.** Compose the simplified univariate functions to obtain closed-form heads  $\hat{\mu}_0(\mathbf{x})$  and  $\hat{\mu}_1(\mathbf{x})$  and thus an explicit  $\hat{\tau}(\mathbf{x})$ , which we also simplify algebraically. These expressions are executable and auditable, and they can be inspected term by term or transported across settings by substituting domain-grounded functions if needed.

At stages (3) and (4) we enforce an accept–reject gate: a structural or symbolic change is kept only if the held-out performance stays within its budget ( $\Lambda_{\text{prune}}, \Lambda_{\text{symb}}$ ); otherwise it is reverted. Practitioners may also choose to *skip* pruning and/or symbolification entirely, yielding a continuum from fully flexible KANs (budgets set to 0) to sparse, fully symbolified formulas (larger budgets). This is crucial in regulated or high-stakes settings: one can freeze the pipeline at the desired interpretability level and document any accuracy impact.

When  $L = 1$  and no MultKAN nodes are used, each head reduces to a Kolmogorov–Arnold Additive Model (KAAM). In this setting, we provide **i) probability radar plots** (PRPs) summarizing each variable’s contribution relative to the average outcome, and **ii) partial dependence plots** (PDPs) showing the variation of the outcome as a function of a single covariate (Almodóvar et al., 2025; Knottenbelt et al., 2024). For deeper KANs or any use of MultKAN nodes, we currently provide only the closed-form expressions; visualization tools for these more complex models are left as future work. A detailed description and examples for KAAM-based plots appear in §C.2.

In summary, the pipeline makes the accuracy–interpretability trade-off *controlled and reproducible*. Budgets ( $\Lambda_{\text{arch}}, \Lambda_{\text{prune}}, \Lambda_{\text{symb}}$ ) bound the deviation from the original predictive performance; every accepted change is logged, and every rejected change is reverted. The procedure is architecture-agnostic, produces executable closed-form  $\hat{\mu}_0(\mathbf{x})$ ,  $\hat{\mu}_1(\mathbf{x})$ , and  $\hat{\tau}(\mathbf{x})$ , and can be halted at any stage depending on the practitioner’s needs. We adopt this protocol across all causalKANs variants and experiments that follow.

## 4.2 CAUSALKANS VARIANTS

We instantiate four canonical architectures, standard baselines in the CATE literature, to enable fair comparisons with prior work. These are representative examples: the same substitution process applies to other causalNNs. Figure 3 shows a schematic view where each block can be a KAN, and §B details specific implementations.

**S-KAN** (*causalKAN for S-Learner*) uses a single KAN to predict outcomes:

$$\hat{\mu}(\mathbf{x}, t) = \text{KAN}(\mathbf{x}, t), \quad \hat{\mu}_0(\mathbf{x}) = \hat{\mu}(\mathbf{x}, 0), \quad \hat{\mu}_1(\mathbf{x}) = \hat{\mu}(\mathbf{x}, 1). \quad (6)$$

With one KAN layer, Eq. 6 reduces to an additive model (KAAM). S-KAN naturally supports continuous treatments, since  $\mu_t(\mathbf{x}, \mathbf{t})$  can be evaluated for  $\mathbf{t} \in \mathbb{R}$ .

**T-KAN** (*causalKAN for T-Learner*) employs two independent KAN heads:

$$\hat{\mu}_0(\mathbf{x}) = \text{KAN}_0(\mathbf{x}), \quad \hat{\mu}_1(\mathbf{x}) = \text{KAN}_1(\mathbf{x}). \quad (7)$$

Each head is updated only with its respective treatment group, using

$$\mathcal{L}_{\text{T-KAN}} = \frac{1}{N} \sum_{i=1}^N \left[ t_i (y_i - \hat{\mu}_1(\mathbf{x}_i))^2 + (1 - t_i) (y_i - \hat{\mu}_0(\mathbf{x}_i))^2 \right] + \mathcal{R}. \quad (8)$$

This setup allows treatment-specific fits but may increase variance due to data splitting. Either head can be restricted to KAAM for maximal simplicity.

**TARKAN** (*causalKAN for TARNet*) first computes a representation vector,

$$\mathbf{z}(\mathbf{x}) = \text{KAN}_z(\mathbf{x}) \in \mathbb{R}^{D_z}, \quad (9)$$

then feeds it to two KAN heads as in T-KAN :

$$\hat{\mu}_0(\mathbf{x}) = \text{KAN}_0(\mathbf{z}(\mathbf{x})), \quad \hat{\mu}_1(\mathbf{x}) = \text{KAN}_1(\mathbf{z}(\mathbf{x})). \quad (10)$$

Training follows the T-style loss Eq. 8, applied after the representation. This design parallels TARNet and relates to Mehendale et al. (2025), though we do not impose explicit distribution-matching on  $\mathbf{z}$ .

**DragonKAN** (*causalKAN for DragonNet*) augments TARKAN with a propensity head:

$$\hat{e}(\mathbf{x}) = \sigma(\text{KAN}_e(\mathbf{z}(\mathbf{x}))), \quad (11)$$

where  $\sigma$  is the sigmoid. Training adds a cross-entropy penalty on  $\hat{e}(\mathbf{x})$  to the outcome losses in Eq. 8, encouraging  $\mathbf{z}$  to capture confounding. We omit targeted regularization layers to preserve formula simplicity, focusing on potential–outcome regression and CATE estimation. Unlike S-KAN, these architectures (T-KAN, TARKAN, DragonKAN) are limited to binary or discrete treatments.

## 5 EXPERIMENTAL EVALUATION

We evaluate *causalKANs* on semi-synthetic benchmarks where ground-truth potential outcomes are available: ACIC 2016 (Dorie et al., 2017) and IHDP (Hill, 2011), settings A and B. Semi-synthetic data allow objective assessment of CATE accuracy despite the fundamental problem of causal inference. We report **i)** the Precision in Estimation of Heterogeneous Effect (PEHE) and **ii)** ATE error. Given test set  $\mathcal{D}_{\text{test}}$ , PEHE is

$$\text{PEHE} = \sqrt{\frac{1}{|\mathcal{D}_{\text{test}}|} \sum_{x_i \in \mathcal{D}_{\text{test}}} (\hat{\tau}(x_i) - \tau(x_i))^2}, \quad (12)$$

and ATE error is  $|\hat{\tau} - \tau|$ , where  $(\hat{\tau}, \tau)$  are the estimated and the real ATE, computed as  $\tau = \frac{1}{|\mathcal{D}_{\text{test}}|} \sum \tau(x)$ . All training details follow §4.

**Datasets.** *IHDP (A/B)*. The Infant Health and Development Program is a widely used semi-synthetic benchmark derived from an observational cohort. Outcomes are generated by known functions of the observed covariates, enabling pointwise ground truth. We use the canonical 100 replications, with setting A (homogeneous effects) and setting B (nonlinear with heterogeneous effects). The feature dimension is  $D=25$  and treatment is binary; the sample size is  $N=747$  with pronounced class imbalance. *ACIC 2016*. We evaluate on selected realizations from the ACIC’16 challenge, which provide  $N \approx 4800$  units with  $D=58$  covariates, binary treatment with covariate-dependent assignment, and nonlinear outcome surfaces. We focus on nonlinear polynomial/exponential regimes (e.g., settings 2/7/26) and use 77 replications per realization.

### 5.1 COMPARISON WITH NEURAL ARCHITECTURES

**Baselines** We benchmark S-/T-KAN, TARKAN, and DragonKAN against their MLP-based counterparts (S-/T-learner, TARNet, DragonNet). We intentionally restrict baselines to neural counterparts to test our central claim—*comparable accuracy with improved interpretability*—rather than to chase leaderboards.

We trained causalNNs with the same hyperparameter budget as causalKANs, modifying depth, number of neurons, activations, regularization and learning rate, and selected the best model based on test loss (we justify this choice in §C.1).

Tab 1 reports PEHE and ATE error per dataset/setting. We assess statistical significance using the Friedman test with Holm-corrected Wilcoxon signed-rank post-hoc comparisons at  $\alpha = 0.05$  (see Demšar (2006); Rainio et al. (2024) for a details on these tests). In the tables, the best-performing model (baseline) is underlined. Models in **bold** are those for which we cannot reject the null hypothesis of equal performance with respect to the baseline ( $p \geq 0.05$ ). A train/val/test split of 80/10/10 was leveraged, as well as early stopping and Adam optimizer (Kingma and Ba, 2014).

We observe from both Tab 1 and Fig. 2 that, across all datasets, there exists at least one instance of causalKAN that is the best model or whose performance is statistically indistinguishable from the best-performing neural model, in the sense that we fail to reject the null hypothesis that the models achieve the same value of the evaluation metric.

## 5.2 INTERPRETABILITY RESULTS

We show here some examples that highlight the interpretability of causalKANs, and we will refer to §C.2 for more examples and details on these representations. We selected randomly one realization of the shown datasets.

**ACIC-7.** We show results for a single layer T-KAN (as it is an additive model, we call it T-KAAM) for ACIC-7, which has been demonstrated very high-performance according to Tab 1. This model yields a function of *heterogeneous* CATE, which is a generalized additive model of the covariates (see §B). In addition to the closed-form CATE, we provide in Fig. 4 (extended in §C.2.1) a *Radar plot (Left)* that compares for two individuals, what is the contribution of each variable to the CATE, compared with the average outcome, and a *PDP (Right)* that represent the curve that defines the variation of the CATE ( $\Delta$  CATE) with a specific feature. In this case, we can observe how  $x_{44}$  increases the CATE w.r.t. the average in individual 10, while it decreases the CATE in individual 11, because the shape of the curve that relates  $x_{44}$  and CATE has a maximum near the value of  $x_{44}$  of individual 10.

**IHDP A.** On the other hand, we can estimate *homogeneous* CATEs with a shallow S-KAN (S-KAAM), which provides closed-form homogeneous treatment effect. In IHDP A, where the known (denoised) ITE is 4 for every individual, we leverage S-KAAM to obtain the value of the causal effect. In Fig. 5 we can observe that the predicted formula has an additive linear term relative to the treatment, which correspond to the CATE (as developed in §B). The contribution of other variables (not causal) can be consulted in §C.2.1. In this case, the CATE can directly be consulted in the formula: 3.74 for the given example.

Table 1: ATE error and PEHE for KAN and MLP across datasets. The baseline (best) according to the Friedman corrected test is underlined, and all models not statistically different are **bolded** ( $\alpha \geq 0.05$  in a paired Wilcoxon corrected test). Values are reported as mean<sub>std</sub>.

| Dataset | Model     | KAN                         |                             | MLP                         |                             |
|---------|-----------|-----------------------------|-----------------------------|-----------------------------|-----------------------------|
|         |           | ATE err                     | PEHE                        | ATE err                     | PEHE                        |
| IHDP A  | S-Learner | <b>0.19</b> <sub>0.35</sub> | <b>0.98</b> <sub>1.03</sub> | <b>0.23</b> <sub>0.47</sub> | 1.04 <sub>1.30</sub>        |
|         | T-Learner | <b>0.13</b> <sub>0.08</sub> | <b>0.62</b> <sub>0.28</sub> | 0.24 <sub>0.27</sub>        | 0.90 <sub>0.51</sub>        |
|         | TarNet    | <b>0.13</b> <sub>0.10</sub> | <b>0.64</b> <sub>0.31</sub> | <b>0.17</b> <sub>0.27</sub> | <b>0.70</b> <sub>0.78</sub> |
|         | DragonNet | <b>0.14</b> <sub>0.10</sub> | <b>0.66</b> <sub>0.35</sub> | <b>0.17</b> <sub>0.27</sub> | <b>0.68</b> <sub>0.77</sub> |
| IHDP B  | S-Learner | 0.37 <sub>0.37</sub>        | 3.01 <sub>0.63</sub>        | 0.32 <sub>0.24</sub>        | 2.63 <sub>0.58</sub>        |
|         | T-Learner | 0.34 <sub>0.27</sub>        | 2.80 <sub>0.44</sub>        | <b>0.25</b> <sub>0.20</sub> | <b>2.06</b> <sub>0.35</sub> |
|         | TarNet    | 0.33 <sub>0.24</sub>        | 2.68 <sub>0.44</sub>        | <b>0.23</b> <sub>0.20</sub> | <b>2.08</b> <sub>0.36</sub> |
|         | DragonNet | <b>0.28</b> <sub>0.22</sub> | <b>2.64</b> <sub>0.44</sub> | <b>0.25</b> <sub>0.21</sub> | <b>2.00</b> <sub>0.34</sub> |
| ACIC 2  | S-Learner | <b>0.20</b> <sub>0.38</sub> | <b>0.20</b> <sub>0.38</sub> | 0.38 <sub>0.44</sub>        | 0.74 <sub>0.38</sub>        |
|         | T-Learner | 0.56 <sub>0.42</sub>        | 1.43 <sub>0.72</sub>        | 1.97 <sub>2.13</sub>        | 7.05 <sub>5.48</sub>        |
|         | TarNet    | 0.25 <sub>0.33</sub>        | 0.78 <sub>0.44</sub>        | 0.36 <sub>0.44</sub>        | 0.96 <sub>0.83</sub>        |
|         | DragonNet | <b>0.21</b> <sub>0.26</sub> | 0.75 <sub>0.33</sub>        | 0.36 <sub>0.44</sub>        | 0.96 <sub>0.82</sub>        |
| ACIC 7  | S-Learner | 0.66 <sub>0.75</sub>        | 4.13 <sub>1.56</sub>        | 0.75 <sub>0.60</sub>        | 4.51 <sub>1.54</sub>        |
|         | T-Learner | <b>0.43</b> <sub>0.43</sub> | <b>3.06</b> <sub>1.18</sub> | 1.37 <sub>2.14</sub>        | 7.05 <sub>6.64</sub>        |
|         | TarNet    | <b>0.42</b> <sub>0.43</sub> | <b>3.06</b> <sub>1.18</sub> | 0.58 <sub>0.50</sub>        | 4.17 <sub>1.47</sub>        |
|         | DragonNet | <b>0.43</b> <sub>0.43</sub> | <b>3.06</b> <sub>1.17</sub> | 0.59 <sub>0.50</sub>        | 4.17 <sub>1.48</sub>        |
| ACIC 26 | S-Learner | <b>0.42</b> <sub>0.45</sub> | 3.23 <sub>1.57</sub>        | 0.75 <sub>0.60</sub>        | 4.51 <sub>1.54</sub>        |
|         | T-Learner | <b>0.36</b> <sub>0.34</sub> | <b>2.80</b> <sub>1.08</sub> | 1.37 <sub>2.14</sub>        | 7.05 <sub>6.64</sub>        |
|         | TarNet    | <b>0.35</b> <sub>0.34</sub> | <b>2.80</b> <sub>1.08</sub> | 0.58 <sub>0.50</sub>        | 4.17 <sub>1.47</sub>        |
|         | DragonNet | <b>0.35</b> <sub>0.34</sub> | <b>2.79</b> <sub>1.08</sub> | 0.59 <sub>0.50</sub>        | 4.17 <sub>1.48</sub>        |

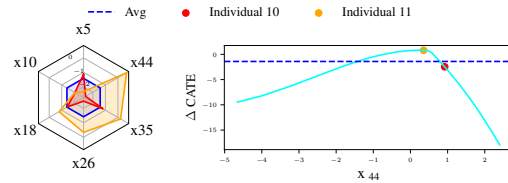
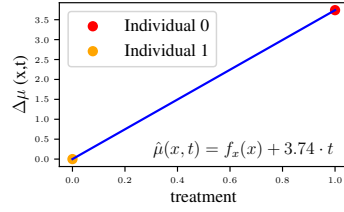


Figure 4: Radar plot and PDP for variable contribution to CATE, using T-KAAM.



**Other datasets.** We omit results for ACIC-26 because they are very similar to those of ACIC-7, while IHDP B and ACIC-2 yield more complex causalKANs, for which we have not explored visualizations. However, we include in §C.2.3 the formulas extracted for one realization of each dataset, which can still be analyzed with function analysis tools.



**Effect of pruning and symbolic substitution in metrics.** For the two previous examples, we show in Fig. 6 how PEHE increases in the pruning and formula substitution steps, while, for the IHDP A dataset, it remains constant in those steps. The actions of completing these steps are controlled by  $\Lambda_{\text{prune}}/\Lambda_{\text{symb}}$ , which measures the MSE and evaluate if we should accept or not the taken step. In this case, we accepted all the steps to give complete interpretability, but the trade-off should be adjusted carefully by the practitioner, since the variations can be high.

We present in §C.2.4 the variation of all the metrics (MSE, ATE and PEHE) for the selected model of each dataset.

These results illustrate that causalKANs can provide closed-form CATE formulas and, in additive cases, complementary visualizations that reveal heterogeneous or homogeneous effects. Importantly, the interpretability pipeline exposes the trade-off between accuracy and simplification, allowing practitioners to adjust it explicitly to their needs.

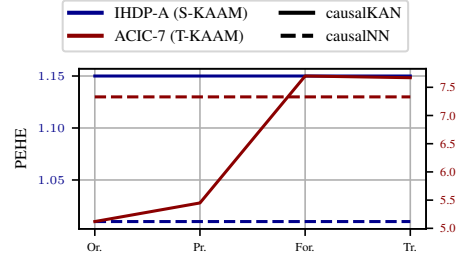


Figure 6: PEHE variation in each step of the pipeline: original (Or.), pruned (Pr.), formula (For.) and 2-decimal truncation (Tr.). Separate axes for each dataset.

## 6 FINAL REMARKS

We have presented causalKANs, a framework that transforms high-performing neural CATE estimators into knowledge-augmented networks with closed-form, auditable effect functions. On standard benchmarks, at least one causalKAN variant matches or surpasses its neural counterpart on PEHE/ATE, while shallow heads (KAAMs) often yield the most favorable accuracy-interpretability trade-off. The pruning and auto-symbolification stages expose explicit formulas and partial dependence plots (PDP; Friedman (2001)). These properties make causalKANs suitable for healthcare, policy evaluation, and economics, where interpretability is central to adoption and auditing (Amann et al., 2020; Doshi-Velez and Kim, 2017; Rudin, 2018; Tonekaboni et al., 2019). Closed-form expressions can be scrutinized, simplified, or aligned with domain-grounded terms to support external validity. We release code to ensure reproducibility and facilitate adoption.

Nevertheless, causalKANs also present open challenges. Visualization tools are currently most effective for shallow KAAMs, while scaling them to deeper or more complex networks remains an area for development. Training and inference are generally more demanding than for standard neural models, and performance can be sensitive to regularization choices or pruning/symbolification budgets, which may introduce approximation errors or variability. As with all observational CATE estimation, our conclusions depend on standard identification assumptions (e.g., unconfoundedness, overlap), and our evaluation relies mainly on semi-synthetic datasets, so further assessment on field data is needed. Finally, uncertainty quantification for symbolic outputs and broader support for continuous or multi-valued treatments are still limited.

Building on these observations, future work should expand theoretical and empirical aspects of causalKANs. Methodologically, interpretability should be assessed with task-grounded and user-study metrics (Tonekaboni et al., 2019), and contrasted with post-hoc explanations such as LIME and SHAP (Lundberg and Lee, 2017; Ribeiro et al., 2016, routinely used but with different guarantees). Developing principled surrogate metrics for model selection, and procedures that reduce accuracy gaps across the simplification stages, would improve stability and reliability. Extending causalKANs to continuous and multi-treatment settings, as well as deriving finite-sample guarantees for CATE

estimation, remain important directions. Incorporating inverse-probability weighting, doubly robust objectives, and batch sampling techniques would further broaden scope. Empirically, validation on real-world data, ideally against interventional or natural experiments, is essential. Beyond PDPs, implementing related plot families, such as accumulated local effects (Apley and Zhu, 2020) or individual conditional expectation (Goldstein et al., 2015), may also be informative when applied directly to the closed-form formulas. Finally, exploring robustness to adversarial perturbations, distribution shifts, and fairness constraints (Rudin, 2018), together with reducing the performance gaps between KAN-ification, pruning, and symbolification, will be important for reliable deployment.

## ACKNOWLEDGEMENTS

The authors of this paper have received the support of the *Synthema* project, funded by European Union’s Horizon Europe, under grant agreement ID 101095530.

## BIBLIOGRAPHY

- R. Agarwal, L. Melnick, N. Frosst, X. Zhang, B. Lengerich, R. Caruana, and G. E. Hinton. Neural additive models: Interpretable machine learning with neural nets. In M. Ranzato, A. Beygelzimer, Y. Dauphin, P. Liang, and J. W. Vaughan, editors, *Advances in Neural Information Processing Systems*, volume 34, pages 4699–4711. Curran Associates, Inc., 2021. (Cited in page 2.)
- A. Al Bataineh, B. Vamsi, M. El-Abd, and B. P. Doppala. Kolmogorov–arnold networks for predicting carotid intima-media thickness in cardiovascular risk assessment. *Scientific Reports*, 15(1):32108, 2025. (Cited in page 2.)
- A. Alaa and M. Schaar. Limits of estimating heterogeneous treatment effects: Guidelines for practical algorithm design. In *International Conference on Machine Learning*, pages 129–138. PMLR, 2018. (Cited in page 3.)
- F. Alharbi, N. Budhiraja, A. Vakanski, B. Zhang, M. Elbashir, H. Guduru, and M. Mohammed. Interpretable graph kolmogorov–arnold networks for multi-cancer classification and biomarker identification using multi-omics data. *Scientific Reports*, 15, 07 2025. doi: 10.1038/s41598-025-13337-0. (Cited in page 2.)
- A. Almodóvar, P. A. Apellániz, A. Garrido, F. Fernández-Salvador, S. Zazo, and J. Parras. Interpretable clinical classification with kolgomorov-arnold networks, 2025. URL <https://arxiv.org/abs/2509.16750>. (Cited in pages 2, 6, 17, and 20.)
- J. Amann, A. Blasimme, E. Vayena, D. Frey, and V. I. Madai. Explainability for artificial intelligence in healthcare: a multidisciplinary perspective. *BMC Medical Informatics and Decision Making*, 20(310), 2020. doi: 10.1186/s12911-020-01332-6. (Cited in pages 1 and 9.)
- D. W. Apley and J. Zhu. Visualizing the effects of predictor variables in black box supervised learning models. *Journal of the Royal Statistical Society: Series B (Statistical Methodology)*, 82(4):1059–1086, 2020. doi: 10.1111/rssb.12377. (Cited in page 10.)
- V. I. Arnold. On functions of three variables. *Doklady Akademii Nauk SSSR*, 114:679–681, 1957. English translation in *American Mathematical Society Translations*, Series 2, Vol. 28: Sixteen Papers on Analysis, 1963, pp. 51–54. (Cited in page 4.)
- S. Athey and G. Imbens. Recursive partitioning for heterogeneous causal effects. *Proceedings of the National Academy of Sciences*, 113(27):7353–7360, 2016. doi: 10.1073/pnas.1510489113. (Cited in page 2.)
- F. J. Bargagli-Stoffi, R. Cadei, K. Lee, and F. Dominici. Causal rule ensemble: Interpretable discovery and inference of heterogeneous treatment effects, 2024. URL <https://arxiv.org/abs/2009.09036>. (Cited in page 3.)
- A. D. Bodner, A. S. Tepsich, J. N. Spolski, and S. Pourteau. Convolutional kolmogorov-arnold networks. *arXiv preprint arXiv:2406.13155*, 2024. (Cited in page 2.)

- 
- J. Braun and M. Griebel. On a constructive proof of kolmogorov’s superposition theorem. *Constructive approximation*, 30(3):653–675, 2009. (Cited in page 4.)
- R. Caruana, Y. Lou, J. Gehrke, P. Koch, M. Sturm, and N. Elhadad. Intelligible models for healthcare: Predicting pneumonia risk and hospital 30-day readmission. In *Proceedings of the 21th ACM SIGKDD international conference on knowledge discovery and data mining*, pages 1721–1730, 2015. (Cited in page 2.)
- K. Chen, Q. Yin, and Q. Long. Covariate-balancing-aware interpretable deep learning models for treatment effect estimation. *Statistics in Biosciences*, 17(1):132–150, April 2025. doi: 10.1007/s12561-023-09394-6. (Cited in page 3.)
- S.-Y. Cho, S. Lee, and H.-G. Kim. Forecasting vix using interpretable kolmogorov-arnold networks. *Expert Systems with Applications*, 294:128781, 2025. ISSN 0957-4174. doi: <https://doi.org/10.1016/j.eswa.2025.128781>. (Cited in page 2.)
- A. Curth and M. Van der Schaar. On inductive biases for heterogeneous treatment effect estimation. *Advances in Neural Information Processing Systems*, 34:15883–15894, 2021a. (Cited in page 4.)
- A. Curth and M. Van der Schaar. Nonparametric estimation of heterogeneous treatment effects: From theory to learning algorithms. In *International Conference on Artificial Intelligence and Statistics*, pages 1810–1818. PMLR, 2021b. (Cited in pages 3 and 4.)
- A. Curth, R. W. Peck, E. McKinney, J. Weatherall, and M. van der Schaar. Using machine learning to individualize treatment effect estimation: Challenges and opportunities. *Clinical Pharmacology & Therapeutics*, 115(4):710–719, 2024. doi: 10.1002/cpt.3159. (Cited in page 1.)
- J. Demšar. Statistical comparisons of classifiers over multiple data sets. *Journal of Machine learning research*, 7(Jan):1–30, 2006. (Cited in page 8.)
- V. Dorie, J. Hill, U. Shalit, M. Scott, and D. Cervone. Automated versus do-it-yourself methods for causal inference: Lessons learned from a data analysis competition, 2017. (Cited in pages 2 and 7.)
- F. Doshi-Velez and B. Kim. Towards a rigorous science of interpretable machine learning. *arXiv: Machine Learning*, 2017. (Cited in pages 2 and 9.)
- European Parliament and Council. Regulation (EU) 2016/679 (GDPR) on the protection of natural persons with regard to the processing of personal data and on the free movement of such data. Official Journal of the European Union, 2016. (Cited in page 1.)
- European Parliament and Council. Regulation (EU) 2024/1689 (Artificial Intelligence Act). Official Journal of the European Union, 2024. Transparency and information requirements for high-risk AI systems. (Cited in page 1.)
- J. C. Foster, J. M. Taylor, and S. J. Ruberg. Subgroup identification from randomized clinical trial data. *Statistics in Medicine*, 30, 2011. (Cited in page 2.)
- D. Frauen and S. Feuerriegel. Estimating individual treatment effects under unobserved confounding using binary instruments. *arXiv preprint arXiv:2208.08544*, 2022. (Cited in page 3.)
- J. H. Friedman. Greedy function approximation: a gradient boosting machine. *Annals of statistics*, pages 1189–1232, 2001. (Cited in pages 9 and 20.)
- A. Goldstein, A. Kapelner, J. Bleich, and E. Pitkin. Peeking inside the black box: Visualizing statistical learning with plots of individual conditional expectation. *journal of Computational and Graphical Statistics*, 24(1):44–65, 2015. (Cited in pages 10 and 20.)
- B. Goodman and S. Flaxman. European union regulations on algorithmic decision-making and a “right to explanation”. *AI magazine*, 38(3):50–57, 2017. (Cited in page 1.)
- P. Hahn, C. Carvalho, D. Puelz, and J. He. Regularization and confounding in linear regression for treatment effect estimation. *Bayesian Analysis*, 13(1):163–182, 2018. ISSN 1936-0975. doi: 10.1214/16-BA1044. Publisher Copyright: © 2018 International Society for Bayesian Analysis. (Cited in page 2.)

- 
- M. A. Hernán and J. M. Robins. *Causal Inference: What If*. CRC Press, Boca Raton, 1st edition, 2025. ISBN 978-0367711337. (Cited in page 3.)
- J. L. Hill. Bayesian nonparametric modeling for causal inference. *Journal of Computational and Graphical Statistics*, 20(1):217–240, 2011. doi: 10.1198/jcgs.2010.08162. (Cited in pages 2 and 7.)
- K. Hornik, M. Stinchcombe, and H. White. Multilayer feedforward networks are universal approximators. *Neural networks*, 2(5):359–366, 1989. (Cited in page 3.)
- K. Imai and A. Strauss. Estimation of heterogeneous treatment effects from randomized experiments, with application to the optimal planning of the get-out-the-vote campaign. *Political Analysis*, 19(1):1–19, 2011. doi: 10.1093/pan/mpq035. (Cited in page 1.)
- F. D. Johansson, U. Shalit, and D. Sontag. Learning representations for counterfactual inference. In *Proceedings of the 33rd International Conference on International Conference on Machine Learning - Volume 48*, ICML’16, page 3020–3029. JMLR.org, 2016. (Cited in page 2.)
- D. M. Kent, E. Steyerberg, and D. van Klaveren. Personalized evidence based medicine: predictive approaches to heterogeneous treatment effects. *BMJ*, 363:k4245, 2018. doi: 10.1136/bmj.k4245. (Cited in page 1.)
- C. Kim and O. Bastani. Learning interpretable models with causal guarantees, 2021. URL <https://arxiv.org/abs/1901.08576>. (Cited in page 3.)
- D. P. Kingma and J. Ba. Adam: A method for stochastic optimization. *CoRR*, abs/1412.6980, 2014. (Cited in page 8.)
- W. Knottenbelt, Z. Gao, R. Wray, W. Z. Zhang, J. Liu, and M. Crispin-Ortuzar. Coxkan: Kolmogorov-arnold networks for interpretable, high-performance survival analysis. *arXiv preprint arXiv:2409.04290*, 2024. (Cited in page 6.)
- A. N. Kolmogorov. On the representation of continuous functions of several variables as superpositions of continuous functions of a smaller number of variables. *Doklady Akademii Nauk SSSR*, 108(2):179–182, 1956. (Cited in page 4.)
- A. N. Kolmogorov. On the representations of continuous functions of many variables by superposition of continuous functions of one variable and addition. In *Dokl. Akad. Nauk USSR*, volume 114, pages 953–956, 1957. (Cited in page 4.)
- S. R. Künnel, J. S. Sekhon, P. J. Bickel, and B. Yu. Metalearners for estimating heterogeneous treatment effects using machine learning. *Proceedings of the national academy of sciences*, 116(10):4156–4165, 2019. (Cited in pages 2, 3, and 4.)
- Y. Ling, P. Upadhyaya, L. Chen, X. Jiang, and Y. Kim. Emulate randomized clinical trials using heterogeneous treatment effect estimation for personalized treatments: Methodology review and benchmark. *Journal of biomedical informatics*, 137:104256, 2023. (Cited in page 4.)
- Z. Liu, P. Ma, Y. Wang, W. Matusik, and M. Tegmark. Kan 2.0: Kolmogorov-arnold networks meet science. *arXiv preprint arXiv:2408.10205*, 2024a. (Cited in pages 1, 4, and 5.)
- Z. Liu, Y. Wang, S. Vaidya, F. Ruehle, J. Halverson, M. Soljačić, T. Y. Hou, and M. Tegmark. Kan: Kolmogorov-arnold networks. *arXiv preprint arXiv:2404.19756*, 2024b. (Cited in pages 1, 2, 4, 5, 21, and 26.)
- J. Loftus, L. Bynum, and S. Hansen. Causal dependence plots. *Advances in Neural Information Processing Systems*, 37:112656–112683, 2024. (Cited in page 20.)
- S. Lolak, J. Attia, G. J. McKay, and A. Thakkinian. Application of dragonnet and conformal inference for estimating individualized treatment effects for personalized stroke prevention: Retrospective cohort study. *JMIR cardio*, 9:e50627, 2025. (Cited in page 4.)
- S. M. Lundberg and S.-I. Lee. A unified approach to interpreting model predictions. In *Advances in Neural Information Processing Systems*, pages 4765–4774, 2017. (Cited in page 9.)

- 
- C. F. Manski. Statistical treatment rules for heterogeneous populations. *Econometrica*, 72(4): 1221–1246, 2004. doi: 10.1111/j.1468-0262.2004.00530.x. (Cited in page 1.)
- E. Mehendale, A. Thorat, R. Kolla, and N. Pedanekar. Kanite: Kolmogorov-arnold networks for ite estimation. *arXiv preprint arXiv:2503.13912*, 2025. (Cited in pages 3 and 7.)
- M. Moradi, S. Panahi, E. Bollt, and Y.-C. Lai. Kolmogorov-arnold network autoencoders, 2024. URL <https://arxiv.org/abs/2410.02077>. (Cited in page 2.)
- R. Moraffah, M. Karami, R. Guo, A. Raglin, and H. Liu. Causal interpretability for machine learning - problems, methods and evaluation. *SIGKDD Explor. Newsl.*, 22(1):18–33, May 2020. ISSN 1931-0145. doi: 10.1145/3400051.3400058. (Cited in page 3.)
- X. Nie and S. Wager. Quasi-oracle estimation of heterogeneous treatment effects. *Biometrika*, 108 (2):299–319, 2021. (Cited in page 3.)
- O. H. M. Padilla, Y. Chen, C. M. M. Padilla, and G. Ruiz. A causal fused lasso for interpretable heterogeneous treatment effects estimation, 2025. URL <https://arxiv.org/abs/2110.00901>. (Cited in page 3.)
- J. Pearl. *Causality*. Cambridge university press, 2009. (Cited in page 20.)
- V. S. Pendyala and N. Venkatachalam. The effectiveness of kolmogorov–arnold networks in the healthcare domain. *Applied Sciences*, 15(16), 2025. ISSN 2076-3417. (Cited in page 2.)
- O. Rainio, J. Teuho, and R. Klén. Evaluation metrics and statistical tests for machine learning. *Scientific Reports*, 14(1):6086, 2024. (Cited in page 8.)
- M. T. Ribeiro, S. Singh, and C. Guestrin. “Why Should I Trust You?” explaining the predictions of any classifier. In *Proceedings of the 22nd ACM SIGKDD International Conference on Knowledge Discovery and Data Mining*, pages 1135–1144, 2016. doi: 10.1145/2939672.2939778. (Cited in page 9.)
- D. B. Rubin. Estimating causal effects of treatments in randomized and nonrandomized studies. *Journal of educational Psychology*, 66(5):688, 1974. (Cited in page 3.)
- C. Rudin. Stop explaining black box machine learning models for high stakes decisions and use interpretable models instead. *Nature Machine Intelligence*, 1:206 – 215, 2018. (Cited in pages 3, 9, and 10.)
- M. J. Saary. Radar plots: a useful way for presenting multivariate health care data. *Journal of clinical epidemiology*, 61(4):311–317, 2008. (Cited in page 19.)
- P. Sanchez, J. P. Voisey, T. Xia, H. I. Watson, A. Q. O’Neil, and S. A. Tsiftaris. Causal machine learning for healthcare and precision medicine. *Royal Society Open Science*, 9(8):220638, 2022. (Cited in page 1.)
- M. Schmidt and H. Lipson. Distilling free-form natural laws from experimental data. *Science*, 324 (5923):81–85, 2009. doi: 10.1126/science.1165893. (Cited in page 2.)
- P. Schwab, L. Linhardt, and W. Karlen. Perfect match: A simple method for learning representations for counterfactual inference with neural networks. *arXiv preprint arXiv:1810.00656*, 2018. (Cited in pages 2 and 4.)
- U. Shalit, F. D. Johansson, and D. Sontag. Estimating individual treatment effect: generalization bounds and algorithms. In *International conference on machine learning*, pages 3076–3085. PMLR, 2017. (Cited in pages 1, 2, 3, and 4.)
- C. Shi, D. Blei, and V. Veitch. Adapting neural networks for the estimation of treatment effects. *Advances in neural information processing systems*, 32, 2019. (Cited in pages 1, 2, and 4.)
- H. Shuai and F. Li. Physics-informed kolmogorov-arnold networks for power system dynamics. *IEEE Open Access Journal of Power and Energy*, 12:46–58, 2025. ISSN 2687-7910. doi: 10.1109/oajpe.2025.3529928. (Cited in page 2.)



- 
- J. Splawa-Neyman, D. M. Dabrowska, and T. P. Speed. On the application of probability theory to agricultural experiments. essay on principles. section 9. *Statistical Science*, pages 465–472, 1990. (Cited in page 3.)
- G. Tesei, S. Giampanis, J. Shi, and B. Norgeot. Learning end-to-end patient representations through self-supervised covariate balancing for causal treatment effect estimation. *Journal of biomedical informatics*, 140:104339, 2023. (Cited in page 3.)
- S. Tonekaboni, S. Joshi, M. D. McCradden, and A. Goldenberg. What clinicians want: Contextualizing explainable machine learning for clinical end use. In *Proceedings of the 4th Machine Learning for Healthcare Conference*, volume 106, pages 359–380. PMLR, 2019. (Cited in pages 1 and 9.)
- M. J. Van der Laan, S. Rose, et al. *Targeted learning: causal inference for observational and experimental data*, volume 4. Springer, 2011. (Cited in page 4.)
- S. Wager and S. Athey. Estimation and inference of heterogeneous treatment effects using random forests. *Journal of the American Statistical Association*, 113(523):1228–1242, 2018. doi: 10.1080/01621459.2017.1319839. (Cited in page 1.)
- H. Wakaura, R. Mulyawan, and A. B. Suksmono. Enhanced variational quantum kolmogorov-arnold network. *arXiv preprint arXiv:2503.22604*, 2025. (Cited in page 2.)
- Y. Wu, H. Liu, K. Ren, S. Ma, and X. Chang. A new causal rule learning approach to interpretable estimation of heterogeneous treatment effect, 2025. URL <https://arxiv.org/abs/2310.06746>. (Cited in page 3.)
- L. Yao, S. Li, Y. Li, M. Huai, J. Gao, and A. Zhang. Representation learning for treatment effect estimation from observational data. *Advances in neural information processing systems*, 31, 2018. (Cited in pages 2 and 4.)
- J. Yoon, J. Jordon, and M. van der Schaar. GANITE: Estimation of individualized treatment effects using generative adversarial nets. In *International Conference on Learning Representations*, 2018. (Cited in page 2.)
- R. C. Yu, S. Wu, and J. Gui. Residual kolmogorov-arnold network for enhanced deep learning. *arXiv preprint arXiv:2410.05500*, 2024. (Cited in page 2.)
- R. Zhang, A. Lensen, and C. Shang. Speeding up genetic programming based symbolic regression using gpus. In *Proc. of EvoApplications*, 2022. (Cited in page 2.)
- Y. Zhang, H. Zhang, Z. C. Lipton, L. E. Li, and E. Xing. Exploring transformer backbones for heterogeneous treatment effect estimation. *Transactions on Machine Learning Research*, 2023. ISSN 2835-8856. (Cited in page 3.)
- Q. Zhao and T. Hastie. Causal interpretations of black-box models. *Journal of Business & Economic Statistics*, 39(1):272–281, 2021. (Cited in page 20.)

# Appendix

## A TREATMENT SPACE GENERALIZATIONS

Let us generalize the theory explained in §3 to the settings of multiple treatment and continuous treatment. CausalKANs can also be generalized following the same fashion.

### A.1 MULTIPLE DISCRETE TREATMENTS

We extend the setup in §3 to  $\mathbf{t} \in \mathcal{T} = \{1, \dots, K\}$ . For each  $k \in \{1, \dots, K\}$ , define the potential outcome  $\mathbf{y}(k)$  and the potential outcome regressor

$$\mu_k(\mathbf{x}) := \mathbb{E}[\mathbf{y}(k) \mid \mathbf{x} = \mathbf{x}]. \quad (13)$$

Pairwise conditional average treatment effects are contrasts

$$\tau_{ba}(\mathbf{x}) := \mu_b(\mathbf{x}) - \mu_a(\mathbf{x}), \quad a, b \in \{1, \dots, K\}. \quad (14)$$

Assumptions generalize in the standard way: (i) positivity,  $P(\mathbf{t} = k \mid \mathbf{x} = \mathbf{x}) > 0$  for all  $k$ ; (ii) conditional ignorability,  $\mathbf{y}(k) \perp\!\!\!\perp \mathbf{t} \mid \mathbf{x}$  for all  $k$ ; (iii) consistency,  $\mathbf{y}_i(t_i) = y_i$ ; and (iv) no interference. Let the propensity vector be  $e_k(\mathbf{x}) = P(\mathbf{t} = k \mid \mathbf{x} = \mathbf{x})$ ,  $\sum_k e_k(\mathbf{x}) = 1$ .

**S-learner (unchanged).** Use a single regressor  $\hat{\mu}(\mathbf{x}, t)$ ; predicted heads are  $\hat{\mu}_k(\mathbf{x}) = \hat{\mu}(\mathbf{x}, k)$ . Train with factual MSE:

$$\mathcal{L}_{\text{S-Learner}} = \frac{1}{N} \sum_{i=1}^N (\hat{\mu}(\mathbf{x}_i, t_i) - y_i)^2. \quad (15)$$

**T-learner ( $K$  heads).** Instantiate  $K$  heads  $\hat{\mu}_k(\mathbf{x})$  and update only the factual head:

$$\mathcal{L}_{\text{T-learner}} = \frac{1}{N} \sum_{i=1}^N (y_i - \hat{\mu}_{t_i}(\mathbf{x}_i))^2. \quad (16)$$

**TARNet ( $K$  heads).** Use a shared representation  $\mathbf{z}(\mathbf{x}) \in \mathbb{R}^{D_z}$  and  $K$  heads:

$$\mathbf{z}(\mathbf{x}), \quad \hat{\mu}_k(\mathbf{z}(\mathbf{x})) = \text{Head}_k(\mathbf{z}(\mathbf{x})), \quad \mathcal{L}_{\text{TARNet}} = \frac{1}{N} \sum_i (y_i - \hat{\mu}_{t_i}(\mathbf{z}(\mathbf{x}_i)))^2. \quad (17)$$

**DragonNet ( $K+1$  heads).** Add a propensity head with softmax output:

$$\hat{e}_k(\mathbf{z}(\mathbf{x})) = \text{softmax}_k(\mathbf{z}(\mathbf{x})), \quad \mathcal{L}_{\text{DragonNet}} = \mathcal{L}_{\text{TARNet}} + \lambda_{PS} \left[ -\frac{1}{N} \sum_i \log \hat{e}_{t_i}(\mathbf{z}(\mathbf{x}_i)) \right]. \quad (18)$$

After training, pairwise CATEs follow from equation 14 with  $\mu_k$  replaced by  $\hat{\mu}_k$ .

### A.2 CONTINUOUS TREATMENTS

Let  $\mathbf{t} \in \mathcal{T} \subset \mathbb{R}$  and define the dose-response function

$$\mu(\mathbf{x}, t) := \mathbb{E}[\mathbf{y}(t) \mid \mathbf{x} = \mathbf{x}]. \quad (19)$$

For any reference level  $t_0 \in \mathcal{T}$ , the conditional effect of moving from  $t_0$  to  $t$  is

$$\tau(\mathbf{x}, t) := \mu(\mathbf{x}, t) - \mu(\mathbf{x}, t_0), \quad (20)$$

and local effects can be summarized by the marginal treatment effect  $\partial\mu(\mathbf{x}, t)/\partial t$  if desired. The identifiability assumptions extend as: positivity w.r.t. the treatment density  $p(t \mid \mathbf{x})$ , conditional ignorability  $\mathbf{y}(t) \perp\!\!\!\perp \mathbf{t} \mid \mathbf{x}$  for all  $t \in \mathcal{T}$ , consistency, and no interference.

**Applicable architecture.** Among the causalNNs above, only the S-learner directly accommodates continuous  $t$ :

$$\mathcal{L}_{\text{S-cont}} = \frac{1}{N} \sum_{i=1}^N (\hat{\mu}(\mathbf{x}_i, t_i) - y_i)^2, \quad (21)$$

with  $\hat{\tau}(\mathbf{x}, t) = \hat{\mu}(\mathbf{x}, t) - \hat{\mu}(\mathbf{x}, t_0)$ .  $\hat{\tau}(\mathbf{x}, t)$  can also be provided directly as a function of the treatment. T-learner/TARNet/DragonNet require finitely many treatment-specific heads and hence are not directly applicable without discretization of  $\mathcal{T}$ ; we therefore recommend the use of the S-learner in continuous-treatment settings.

## B DETAILS ON CAUSALKANS VARIANTS

As explained in §4, the adaptation of causalNNs to causalKANs consists of changing the MLP backbones by KANs. In Fig. 7, we include examples of the proposed causalKANs, with an arbitrary number of layers and summation nodes.

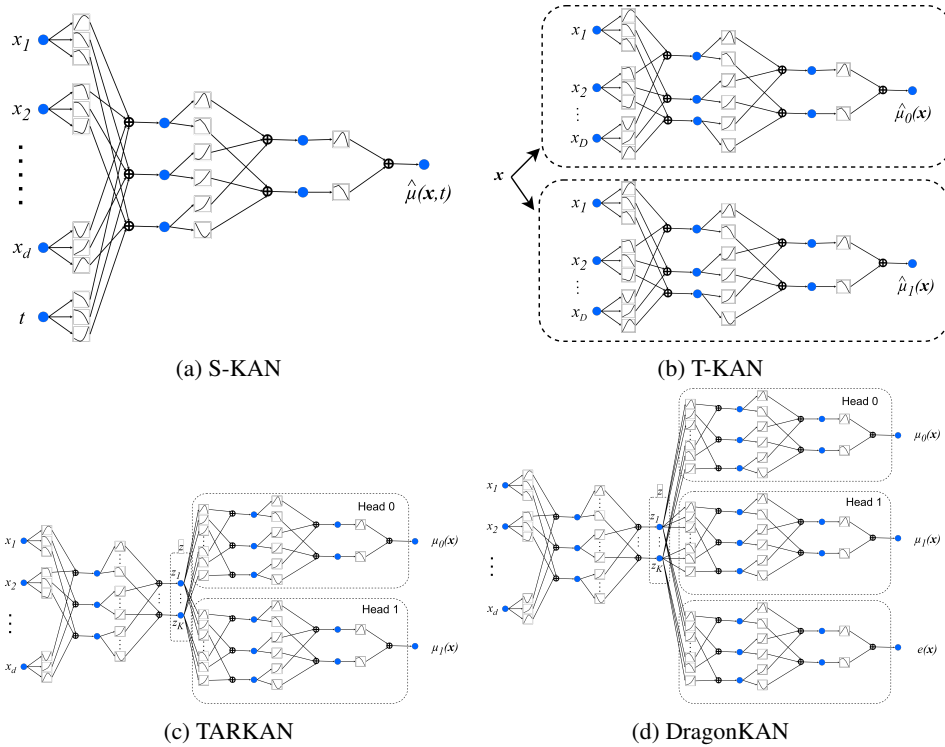


Figure 7: CausalKANs detailed architectures. The number of layers of each model is arbitrary, just to show an example of each one.

From the point of view of interpretability, constructing very complex causalKANs is harmful for achieving simple and auditable formulas. Therefore, as mentioned in point 2 of §4.1, obtain the simplest model is crucial to improve interpretability, and we recommend to minimize the complexity of the network, among the models with similar performance.

We want to illustrate some interesting combinations of hyperparameters, that yield into special interpretable causal effects. In particular, when meta-learners employ additive models, we call them S-KAAM and T-KAAM, and when the heads of TARKAN and DragonKAN are also shallow additive models, we call them TARKAAM and DragonKAAM.

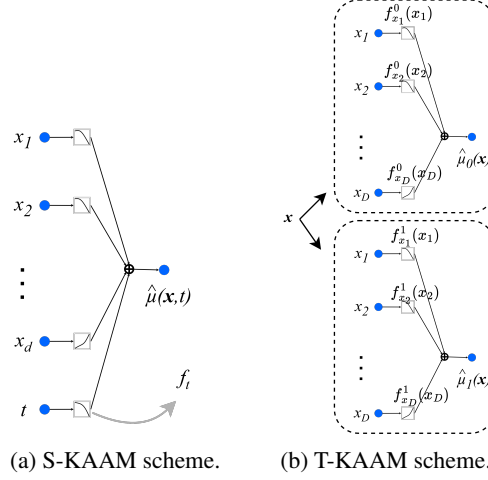


Figure 8: Particularly interpretable architectures of causalKANs.

**S-KAAM.** When training and S-KAN, if the hyperparameters selected results into a single-layer KAN, then we have a KAAM (Almodóvar et al., 2025). We call this model S-KAAM, and a scheme can be found in Fig. 8a. The interesting point is that, when we have an S-KAAM, the effects on the population are homogeneous, and we have access to the *effect curve* directly. The effect curve defines how the outcome varies with the treatment. Since, in a S-KAAM, the model is additive:

$$\hat{\mu}(\mathbf{x}, t) = f_{\mathbf{x}}(\mathbf{x}) + f_t(t), \quad (22)$$

we define the *effect curve*,  $f_t : \mathcal{T} \rightarrow \mathbb{R}$ , as the function that represents the variations of the outcome, depending on the treatment. Therefore, any causal effect of two different values of the treatment,  $a, b$  can be computed as the difference along the effect curve:

$$\hat{\tau}_{ab}(\mathbf{x}) = \hat{\mu}(\mathbf{x}, b) - \hat{\mu}(\mathbf{x}, a) = [f_{\mathbf{x}}(\mathbf{x}) + f_t(b)] - [f_{\mathbf{x}}(\mathbf{x}) + f_t(a)] = f_t(b) - f_t(a), \quad (23)$$

Note that this model yields homogeneous treatment effects, making the CATE equivalent to the ATE, and removing the covariate dependence.

For a binary treatment, the CATE can be computed as:

$$\hat{\tau}(\mathbf{x}) = f_t(1) - f_t(0), \quad (24)$$

**T-KAAM.** In the same fashion, if both subnetworks in a T-KAN are KAAMs, we can get a simple analytic solution of the causal effect, that depends on each covariate independently.

Having that each potential outcome can be expressed as:

$$\hat{\mu}_t(\mathbf{x}) = f_{x_1}^t(x_1) + f_{x_2}^t(x_2) + \dots + f_{x_D}^t(x_D), \quad (25)$$

where  $f_{x_i}^t$  is the activation function corresponding to the covariate  $x_i$  in the subnetwork of the treatment  $t$ . We can compute the individual contribution of each variable, yielding in an estimation of the causal effect, for a binary treatment, as:

$$\hat{\tau}(\mathbf{x}) = \underbrace{[f_{x_1}^1(x_1) - f_{x_1}^0(x_1)]}_{\mathbf{g}_{x_1}(x_1)} + \underbrace{[f_{x_2}^1(x_2) - f_{x_2}^0(x_2)]}_{\mathbf{g}_{x_2}(x_2)} + \dots + \underbrace{[f_{x_D}^1(x_D) - f_{x_D}^0(x_D)]}_{\mathbf{g}_{x_D}(x_D)} \quad (26)$$

As an implementation detail, note that a T-KAAM can be implemented with a single KAN shallow model with two outputs, each one for  $\hat{\mu}_1(\mathbf{x})$  and  $\hat{\mu}_0(\mathbf{x})$ , respectively.

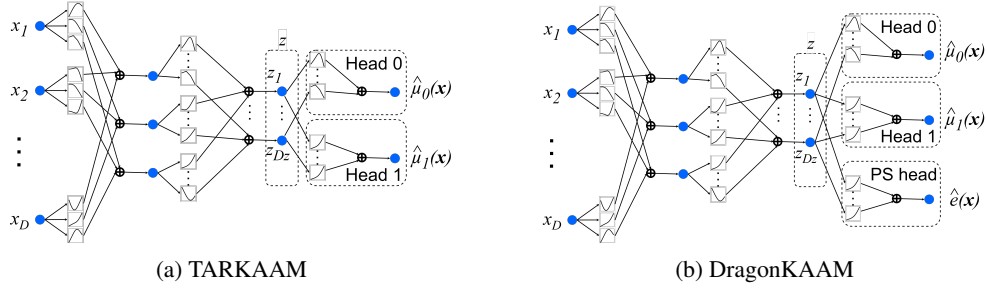


Figure 9: TARKAN and DragonKAN with shallow heads. With respect to Fig. 7, the connections that depart from  $\mathbf{z}$  have been reordered to make the equivalence more noticeable.

**TARKAAM and DragonKAAM.** We would like to make an observation on the implementation of TARKAN and DragonKAN when the heads are shallow KAAMs. We can observe in Fig. 9 that, when instantiating a single KAN, with 2 and 3 output nodes, respectively. To construct those figures, we have reordered the last layer of a single KAN with 2/3 outputs, and show that is equivalent to add 2/3 KAAMs that have  $\mathbf{z}(x)$  as input.

That is an interesting fact because we find, empirically, that TARKAAM and DragonKAAM are between the best-performer TAR-like and Dragon-like networks when evaluating in the IHDP and ACIC datasets. We also note that a KAN can learn identity splines, which could lead to have a representation vector equal to the input:  $\mathbf{z}(x) = \mathbf{x}$ . If that is the case, the TARKAAM and DragonKAAM can be seen as T-KAAMs, since all the outputs are independent additive functions of the covariates (except for the common regularization term,  $\mathcal{R}$ ). For example, that is the case for the dataset ACIC-7, which cause that T-KAN, TARKAN and DragonKAN to have the almost same metrics.

## C DETAILED RESULTS

### C.1 ABLATION STUDIES

**Complexity.** We further analyze the relationship between model complexity and the precision in estimation of heterogeneous effects (PEHE). To this end, we define a *complexity score* that aggregates the contributions of different architectural and regularization choices. Specifically, hidden dimensions contribute 0 if no hidden layers are used, 2 if a single hidden layer of size 5 is used, and 3 otherwise. The weight penalty  $\lambda$  contributes 1 if set to 0.01 and 2 otherwise. The spline grid contributes 1, 2, or 3 for grid sizes  $\{1, 3, 5\}$ , respectively. Similarly, the polynomial order  $k$  contributes 1, 2, or 3 for  $k \in \{1, 3, 5\}$ , and sparse initialization reduces the score by one unit. Hence, the complexity score captures the combined effect of the number of hidden units, regularization strength, spline resolution, polynomial order, and initialization strategy. In addition, we compute the number of hidden layers directly from the hidden dimensions: 0 layers (no hidden units, corresponding to KAAM), 1 layer (single hidden layer), and 2 layers (deeper networks).

We then represent the correlation between both complexity and number of hidden layers against PEHE, using linear regression fits and Pearson correlation coefficients across all hyperparameter configurations (Figs. 10 and 11). The results indicate that the correlation is weak: the fitted slopes are close to zero and the Pearson coefficients are generally small. Interestingly, increasing the number of hidden layers often leads to slightly higher PEHE values, although the effect is minor and not consistent across all datasets. Similarly, increasing the overall complexity score does not systematically reduce PEHE.

These findings suggest that, in general, simple KAN architectures achieve competitive PEHE performance, and that increasing architectural or regularization complexity does not yield clear improvements.

**Hyperparameter selection with Loss.** We want to show that the predictive test loss (i.e. the loss of the KAN model without including sparsity regularizations) is a good proxy for selecting hyperparameters, since the PEHE cannot be computed during evaluation because the real ITE is not known in real-world data and can only be computed with (semi)synthetic data. We can observe in



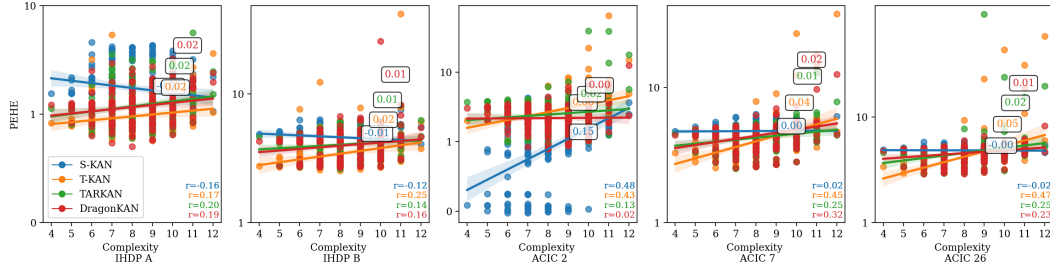


Figure 10: Correlation between model complexity and PEHE across datasets. Each point corresponds to a trained model with a given complexity score. Regression fits (with slopes annotated) and Pearson correlation coefficients are shown. The weak correlations indicate that increasing complexity does not improve PEHE.

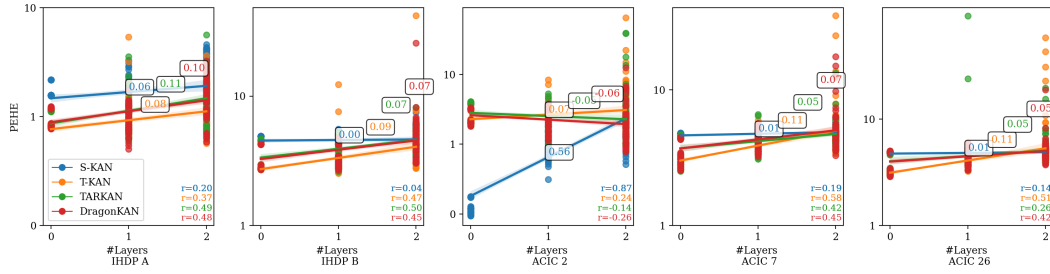


Figure 11: Correlation between the number of hidden layers and PEHE across datasets. The number of layers is computed from the hidden dimensions: 0 (no hidden layers, i.e., KAAM), 1 (single hidden layer), and 2 (two hidden layers). Regression fits and Pearson correlations show that deeper models tend to slightly increase PEHE, although the effect is minor.

Fig. 12 that these quantities are linearly correlated. However, the study of other surrogate metrics for model selection is still a topic for future work.

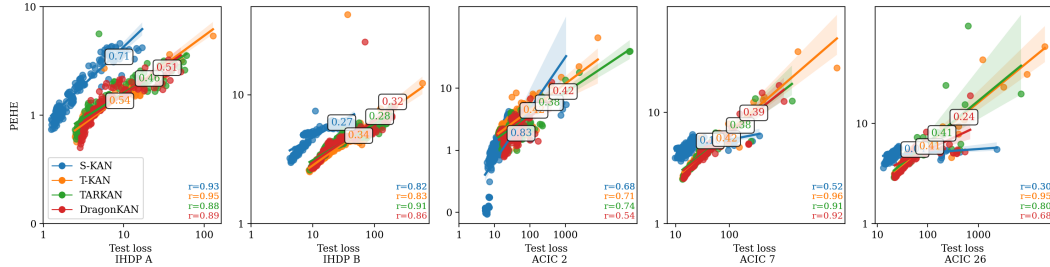


Figure 12: Regression plots of PEHE and Test predictive loss (logarithmic scale) for each dataset with all causalKANs. Slope (in boxes), Pearson coefficient,  $r$ , (in bottom right corners) and 95% CI (translucent bands) reported. We can observe a clear linear correlation between PEHE and Test loss for all models and all datasets.

## C.2 INTERPRETABILITY VISUALIZATIONS

First of all, let us explain in detail the different visualization tools, in addition to the formula analysis *per se*, that will help us to understand outcome variations, depending of the model used.

**Probability Radar Plots (PRPs).** Probability Radar Plots (PRPs) (Saary, 2008) provide an interpretable visualization of generalized additive models (GAMs) by mapping the isolated contribution of each covariate into a radial plot. In our setting, each component function depends on a single

covariate, which enables a decomposition of the prediction into additive terms. We denote this decomposition by  $\Delta$ .

$$\Delta = \begin{bmatrix} f_{x_{1,1}} & f_{x_{1,2}} & \cdots & f_{x_{1,D}} \\ f_{x_{2,1}} & f_{x_{2,2}} & \cdots & f_{x_{2,D}} \\ \vdots & \vdots & \ddots & \vdots \\ f_{x_{N,1}} & f_{x_{N,2}} & \cdots & f_{x_{N,D}} \end{bmatrix}, \quad (27)$$

where  $f_{x_{i,j}}$  denotes the contribution of the feature  $j$  for individual  $i$ .

To construct a PRP, we first compute the average contribution of each covariate across all individuals, providing a baseline that reflects the average outcome (for S-KAAM) or the average conditional average treatment effect (for T-KAAM). Then, for a given individual  $i$ , we plot the vector of deviations

$$(f_{x_{i,1}} - \frac{1}{N} \sum_{\ell=1}^N f_{x_{\ell,1}}, \dots, f_{x_{i,D}} - \frac{1}{N} \sum_{\ell=1}^N f_{x_{\ell,D}}), \quad (28)$$

which highlights how the contribution of each covariate for individual  $i$  differs from the population average. By arranging these deviations radially, PRPs enable intuitive comparison across covariates and between individuals.

**Partial dependence plots (PDPs).** We employ partial dependence plots (PDPs) (Friedman, 2001) as visualization tools for interpreting causalKANs. Unlike their conventional use in a “black-box” fashion—where the model is queried without access to its internals—KAN-based PDPs (Almodóvar et al., 2025) directly exploit the analytic equations of the learned model, displaying the underlying splines that constitute the predictors. This provides more faithful and transparent representations of the learned dependencies.

As noted by Loftus et al. (2024), PDPs that vary one covariate in isolation may be misleading in settings with mediators, since they ignore induced changes in other covariates. In our case, however, the assumptions in §3 guarantee that the covariates form a valid adjustment set, excluding mediators. Under these conditions, PDPs are valid tools to represent causal dependencies (Zhao and Hastie, 2021), and in fact rely on the same backdoor adjustment formula (Pearl, 2009) when the effect is homogeneous.

Formally, PDPs display the average variation in the predicted outcome as one covariate is varied, marginalizing over the remaining covariates. Their individual-level counterpart, individual conditional expectation (ICE) curves (Goldstein et al., 2015), provide counterfactual explanations for specific samples. Under additivity, PDPs and ICE coincide; under non-additivity, PDPs correspond to averages of the heterogeneous ICE curves.

### C.2.1 HETEROGENEOUS CATE WITH T-KAAM

We show an example of how T-KAAM captures the CATE as a closed formula that can be interpreted. For the dataset *ACIC 7*, the T-KAAM model is one of the best-performers, and we can observe that the CATE can be represented as an addition of functions of each variable independently (see Eq. 25). An example obtained with one realization of the dataset can be observed in the following equation.

$$\begin{aligned}
\hat{\tau}(\mathbf{x}) = & 0.09 x_1^2 + 0.19 x_1 - 0.74 x_{10}^2 + 5.30 x_{10} + 0.01 x_{12}^3 - 0.05 x_{12}^2 - 0.09 x_{12} \\
& + 0.03 x_{13}^3 - 0.13 x_{13}^2 - 0.21 x_{13} - 0.06 x_{14}^2 + 0.33 x_{14} - 0.06 x_{15}^2 + 0.13 x_{15} \\
& + 0.19 x_{16}^2 - 0.22 x_{16} - 0.59 x_{17} - 0.03 x_{18}^3 - 0.14 x_{18}^2 - 0.47 x_{18} \\
& + 0.03 x_{19}^4 - 0.10 x_{19}^3 - 0.33 x_{19}^2 + 0.42 x_{19} + 0.14 x_{20}^3 - 0.29 x_{20}^2 - 0.30 x_{20} \\
& + 0.01 x_{21}^3 + 0.05 x_{21}^2 + 0.28 x_{21} + 0.25 x_{23}^3 - 0.50 x_{23}^2 - 0.83 x_{23} - 0.16 x_{24} \\
& - 0.07 x_{25}^2 + 0.14 x_{25} - 1.42 x_{26} - 0.01 x_{27}^4 + 0.04 x_{27}^3 - 0.06 x_{27}^2 + 0.06 x_{27} \\
& - 0.12 x_{28}^2 - 0.32 x_{28} + 0.00 x_{29}^4 + 0.08 x_{29}^3 + 0.07 x_{29}^2 + 0.01 x_{29} \\
& - 0.16 x_3 - 0.17 x_{30} - 0.01 x_{31}^2 - 0.08 x_{31} + 0.54 x_{33} \\
& - 0.03 x_{34}^2 - 0.17 x_{34} + 0.02 x_{35}^3 + 0.23 x_{35}^2 + 0.84 x_{35} \\
& + 0.03 x_{36}^3 - 0.14 x_{36}^2 + 0.22 x_{36} - 0.30 x_{38} - 0.15 x_{39}^2 - 0.20 x_{39} \\
& - 0.03 x_4^2 + 0.12 x_4 - 0.13 x_{40}^3 - 0.31 x_{40}^2 - 0.18 x_{40} \\
& + 0.04 x_{41}^3 - 0.39 x_{41}^2 + 0.02 x_{41} + 0.25 x_{42}^2 + 0.18 x_{42} \\
& + 0.01 x_{43}^4 - 0.03 x_{43}^3 - 0.09 x_{43}^2 + 0.08 x_{43} \\
& - 0.41 x_{44}^3 - 2.42 x_{44}^2 - 0.92 x_{44} - 0.06 x_{45}^3 - 0.29 x_{45}^2 - 0.32 x_{45} \\
& - 0.09 x_{46}^2 - 0.04 x_{46} - 1.10 x_{49} - 0.10 x_5^4 + 0.56 x_5^3 + 1.27 x_5^2 - 1.30 x_5 \\
& - 0.02 x_{50}^2 + 0.01 x_{50} - 0.12 x_{51} + 0.14 x_{52}^2 - 0.71 x_{52} - 0.57 x_{53} + 0.42 x_{54} \\
& - 0.02 x_{56}^3 + 0.01 x_{56}^2 + 0.52 x_{56} - 0.02 x_{57}^3 + 0.09 x_{57}^2 + 0.23 x_{57} \\
& - 0.02 x_{58}^3 - 0.17 x_{58}^2 - 0.34 x_{58} - 0.06 x_7^2 + 0.41 x_7 - 0.21 x_8 + 0.21 x_9^2 - 0.25 x_9 \\
& + 9.47.
\end{aligned}$$

This formula is long, due to the high number of covariates. Therefore, although the contribution of each variable has a polynomial form, analyzing the formula alone could be tricky. To help to gain intuitions about the contribution of each variable to the CATE variation, we present three useful plots in Fig. 13. In the plots, we can obtain the contributions of each feature to the causal effect. However, those visualizations should not be used to intervene in any feature except the treatment, since the variations presented in Fig. 13 cannot be interpreted as causal effect following our assumptions.

Lastly, we want to show that our *inductive bias* for simplicity of the atom selection is useful to improve interpretability. The formula below is provided by the standard auto-symbolic function (native of pyKAN (Liu et al., 2024b)). We observe polynomial relations with some covariates, but the nonlinear complex functions that follow are less interpretable than simple polynomials.

$$\begin{aligned}
\hat{\tau}(\mathbf{x}) = & -0.59 x_{17} - 0.16 x_{20} + 0.26 x_{21} - 1.41 x_{26} + 0.10 x_{27} + 0.28 x_{29} \\
& - 0.25 x_{31} + 0.54 x_{33} + 0.15 x_{34} + 0.34 x_{35} + 0.22 x_{36} - 0.30 x_{38} \\
& - 0.32 x_{40} + 0.02 x_{43} - 1.67 x_{44} - 0.40 x_{45} + 0.65 x_5 - 0.12 x_{51} \\
& - 0.57 x_{53} + 0.42 x_{54} - 0.02 x_{55} - 0.40 x_{58} \\
& - 0.00 (1.17 - 9.05 x_{50})^2 + 0.01 (3.95 - 3.98 x_{16})^2 \\
& - 0.00 (5.62 - 7.80 x_{41})^2 - 0.19 (6.55 - 1.78 x_{10})^2 \\
& - 0.02 (7.66 - 2.42 x_{10})^2 + 0.01 (9.47 - 3.82 x_{52})^2 \\
& + 0.00 (9.80 - 4.97 x_{46})^2 + 0.00 (-2.05 x_{16} - 5.95)^2 \\
& - 0.00 (-9.30 x_{23} - 2.38)^2 + 0.12 \sqrt{5.29 x_{31} + 2.54} \\
& - 0.00 (-8.38 x_{39} - 5.79)^2 - 1.03 \exp(0.60 x_{18}) - 0.23 \exp(0.97 x_{24}) \\
& - 0.53 \exp(0.56 x_{34}) + 0.47 \exp(0.87 x_{35}) + 1.12 \sin(0.63 x_1 - 7.20) \\
& - 0.40 \sin(0.81 x_1 - 0.81) - 0.24 \sin(4.88 x_{12} + 1.30) \\
& - 0.40 \sin(0.83 x_{13} - 1.02) + 1.09 \sin(5.19 x_{13} + 5.19) \\
& - 0.33 \sin(1.81 x_{14} + 2.36) + 2.42 \sin(9.01 x_{15} + 7.79) \\
& - 0.56 \sin(1.35 x_{19} - 2.19) - 0.26 \sin(1.14 x_{20} + 1.39)
\end{aligned}$$

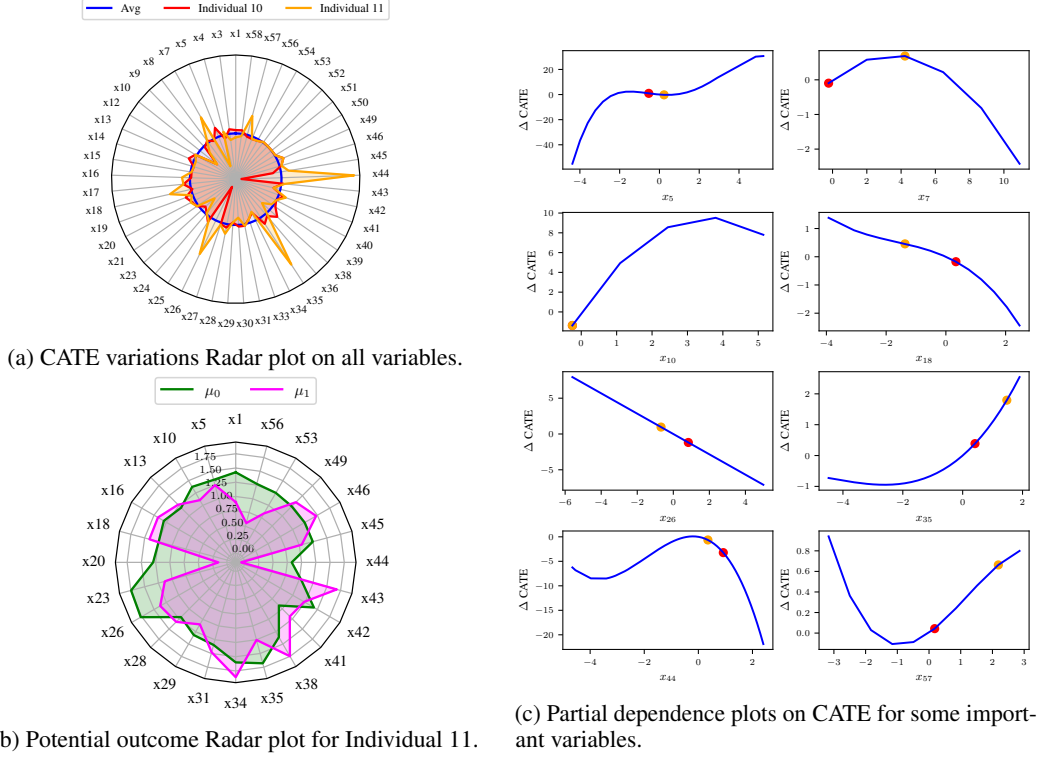


Figure 13: Visualization plots employing T-KAAM with ACIC-7. **(a)** *Radar plot* of the contribution of each variable to the CATE. In **blue**, the average predicted CATE in all the dataset. In **red** and **orange**, the respective contributions of each variable of individuals 10 and 11. **(b)** *Radar plot* of the potential outcomes of the individual 10. We can observe the contribution of each variable to the potential outcomes. Only the variables that have not been pruned in both subnetworks have been added to the plot. **(c)** *Partial dependence plots* of the CATE variation, given variations on the most important variables in the PRP. Particular values of CATE variation for the individuals 10 and 11 shows their contribution.

$$\begin{aligned}
& + 0.51 \sin(1.80 x_{23} - 10.00) - 0.50 \sin(0.63 x_{25} - 8.42) \\
& - 0.86 \sin(0.48 x_{28} - 4.36) + 2.25 \sin(0.52 x_{28} + 1.99) \\
& + 1.09 \sin(0.22 x_3 + 8.43) - 1.02 \sin(4.20 x_{30} + 1.41) \\
& + 0.58 \sin(7.77 x_{41} - 3.80) + 0.74 \sin(1.04 x_{42} - 8.42) \\
& + 0.75 \sin(5.35 x_{42} + 0.85) + 1.29 \sin(9.59 x_{46} + 3.61) \\
& + 0.53 \sin(4.58 x_{49} + 2.43) - 4.78 \sin(4.79 x_{49} - 0.60) \\
& + 0.88 \sin(4.21 x_{56} + 7.78) - 1.94 \sin(5.59 x_{56} - 7.58) \\
& + 0.41 \sin(0.88 x_{57} - 7.16) + 1.03 \sin(3.20 x_7 + 7.20) \\
& + 0.72 \sin(0.40 x_8 + 2.00) + 1.07 \sin(9.06 x_9 + 1.76) \\
& + 0.53 \tanh(0.98 x_{18} - 1.40) + 7.14 - 0.11 \exp(-0.93 x_4) .
\end{aligned}$$

### C.2.2 HOMOGENEOUS CATE WITH S-KAAM

In this section, we illustrate how we obtain the *homogeneous* CATE (or, equivalently, the ATE) in the IHDP A dataset, where the causal effect of the treatment is known to be homogeneous and linear.

Therefore, we instantiate an S-KAAM, which yields the following formula in the potential outcome estimation.

$$\begin{aligned}
\hat{\mu}(\mathbf{x}, t) = & \underline{3.74t} + 0.53 x_1 + 0.16 x_{10} + 0.59 x_{11} - 0.11 x_{12} + 0.34 x_{13} + 0.11 x_{16} - 0.17 x_{18} + 1.28 x_{19} \\
& + 0.01 x_2^3 - 0.01 x_2^2 - 0.23 x_{20} - 0.08 x_{21} + 0.11 x_{24} + 0.18 x_3^2 + 1.29 x_3 + 0.28 x_5
\end{aligned}$$

$$+ 0.01 x_6^4 - 0.03 x_6^3 + 0.03 x_6 + 1.47 x_8 + 0.32 x_9 + 1.88.$$

As presented in Eq. 24, the CATE can be computed exclusively with the terms relative to  $t$ . In this case, the CATE can be directly extracted from the formula: 3.74.

We also represent in Fig. 14 some visualizations that we find interesting. First, for two given individuals, we present a PRP with the contribution of each variable to the variation of the predicted outcome,  $\hat{\mu}(x, t)$ , compared with the average of the predicted outcomes,  $\mathbb{E}_{x,t}[\hat{\mu}(x, t)]$ . On the right, we present the predicted potential outcomes for a given individual. As the effect is homogeneous (does not depend on the covariates), the contribution of each feature for both potential outcomes is the same, and the only difference is the causal effect of the treatment. Lastly, we present PDPs for treatment and other three variables (based on the radar plot), which present the variations of the predicted outcome with each variable. Following our assumptions, only the treatment curve can be seen as a causal effect, while the other curves can be used only to gain intuition of outcome behavior.

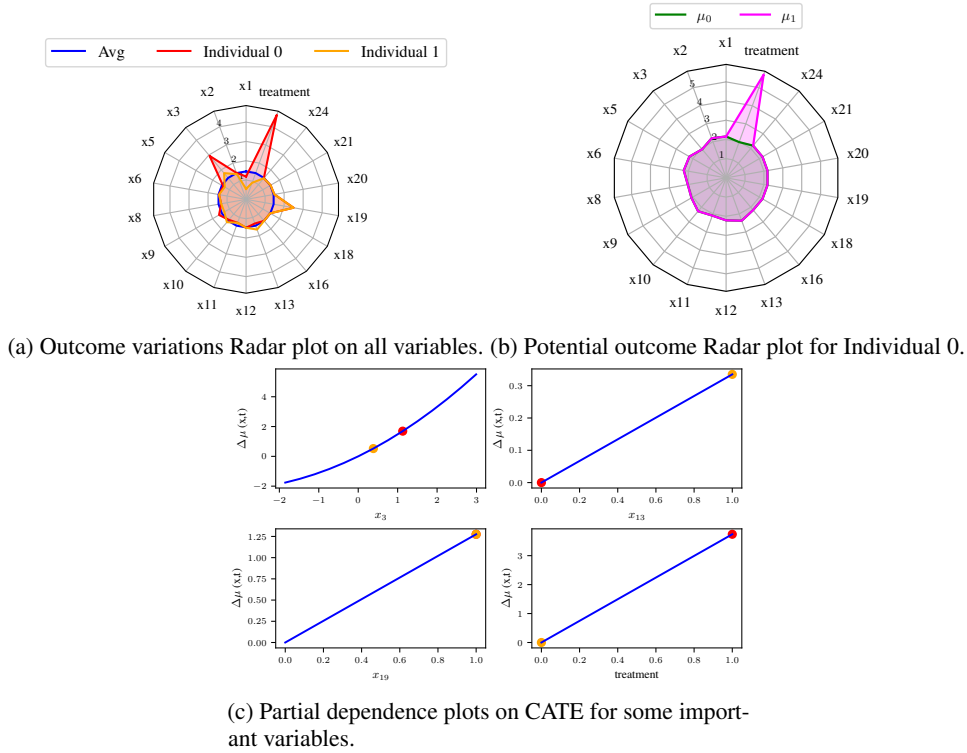


Figure 14: Visualization plots employing S-KAAM with IHDP A. (a) *Radar plot* of the contribution of each variable to the outcome. In blue, the average predicted outcome in all the dataset. In red and orange, the respective contributions of each variable of individuals 0 and 1. (b) *Radar plot* of the potential outcomes of the individual 0. We can observe the contribution of each variable to the potential outcomes. (c) *Partial dependence plots* of the outcome variation, given variations on the most important variables in the PRP. Particularized for the individuals 0 and 1.

In this case, the standard symbolic substitution provides a similar formula as our proposal, due to the linearity of the dataset, and we omit its expression.

### C.2.3 FORMULA EXTRACTION FOR OTHER DATASETS

For the ACIC-2 and IHDP B datasets, we carried out all the process of the pipeline. We can analyze the formula yielded by the process, but visualization tools for interaction terms need still to be developed.



---

Here, we include the extracted CATE formula from DragonKAAM in IHDP B. Unfortunately, the extracted formula is too complex to be analyzed directly. We obtained a similar formula for the dataset ACIC-2, and we omit the presentation of the formula.

$$\begin{aligned}
\hat{\tau}(\mathbf{x}) = & 0.03 x_1 + 0.89 x_{10} - 0.64 x_{11} - 0.78 x_{12} + 0.51 x_{13} + 0.11 x_{14} - 0.89 x_{15} - 0.69 x_{16} - 0.71 x_{17} \\
& - 0.89 x_{18} - 1.55 x_{19} + 0.61 x_2 + 0.07 x_{20} - 1.36 x_{21} + 0.31 x_{22} - 1.50 x_{24} + 0.85 x_{25} - 0.18 x_6 \\
& + 1.14 x_7 + 1.54 x_8 - 0.38 x_9 \\
& - 0.91 \left( 0.02 x_2 - 0.15 x_{21} + 0.04 x_5 - 0.03 x_6 - 0.13 \sin(0.68 x_3 - 7.58) - 0.45 \right) \\
& \left( 0.33 x_{14} + 0.21 x_{21} - 0.65 x_{22} - 0.14 x_5 - 0.20 x_7 - 0.27 x_8 + 0.20 \sin(4.58 x_4 - 2.41) \right. \\
& \left. - 0.18 \tanh(1.02 x_1 - 0.93) - 0.24 \right) \\
& - 0.30 \left( 0.37 x_{11} - 0.42 x_{20} + 0.25 x_{21} + 0.37 x_{24} - 0.31 x_7 + 0.35 \tanh(0.78 x_5 - 1.03) + 0.56 \right) \\
& \times \left( -0.19 x_{11} - 0.23 x_{14} - 0.24 x_{21} - 0.40 x_{24} + 0.20 x_7 - 0.14 \sin(0.97 x_3 + 5.20) \right. \\
& \left. - 0.49 \sin(6.42 x_4 - 2.19) - 0.40 \tanh(0.51 x_5 - 0.70) - 1.15 \right) \\
& - 0.20 \left( 0.22 x_{10} + 0.10 x_{12} + 0.23 x_{14} + 0.51 x_{15} + 0.20 x_{16} + 0.18 x_{17} - 0.06 x_{19} + 0.21 x_{21} \right. \\
& + 0.25 x_{22} - 0.07 x_{24} + 0.15 x_{25} + 0.32 x_7 + 0.18 x_9 - 0.49 \sin(0.58 x_1 + 2.58) \\
& + 0.24 \sin(0.81 x_2 - 0.79) + 0.38 \sin(0.69 x_5 + 5.01) + 1.69 \sin(0.23 x_6 - 7.34) \\
& - 0.10 \tan(2.58 x_4 + 6.01) + 3.35 \left( 0.06 x_1 + 0.18 x_{10} + 0.18 x_{11} + 0.09 x_{12} + 0.08 x_{13} \right. \\
& + 0.09 x_{14} + 0.52 x_{15} + 0.34 x_{17} + 0.21 x_{18} + 0.06 x_{19} + 0.08 x_{22} + 0.35 x_{25} + 0.02 x_3 + 0.14 x_7 \\
& + 0.13 x_8 + 0.06 x_9 + 0.00 (-3.38 x_6 - 8.92)^2 - 0.12 \sin(0.73 x_2 + 8.56) \\
& \left. + 0.58 \sin(0.76 x_5 + 5.39) - 0.11 \tan(8.61 x_4 - 4.40) + 1.54 \right) \\
& - 0.04 \left( 0.14 x_{10} + 0.08 x_{11} + 0.09 x_{12} + 0.15 x_{13} - 0.18 x_{14} - 0.05 x_{15} - 0.22 x_{17} \right. \\
& + 0.13 x_{19} + 0.21 x_{20} - 0.09 x_{21} + 0.31 x_{22} - 0.31 x_{25} - 0.05 x_5 + 0.22 x_8 - 0.14 x_9 \\
& - 0.01 (-1.48 x_1 - 1.91)^2 - 0.01 (-2.04 x_6 - 6.95)^2 - 1.78 \sin(0.23 x_2 + 5.02) \\
& + 1.02 \sin(0.43 x_3 - 4.16) - 0.16 \sin(0.63 x_4 + 8.60) - 2.44 \left. \right) \\
& \times \left( 0.04 x_{10} + 0.13 x_{11} - 0.22 x_{12} + 0.05 x_{13} + 0.32 x_{15} + 0.17 x_{17} + 0.14 x_{19} \right. \\
& - 0.24 x_{20} + 0.14 x_{21} - 0.47 x_{22} - 0.20 x_{23} - 0.11 x_{24} + 0.30 x_{25} - 0.22 x_8 + 0.06 x_9 \\
& + 0.15 \sin(0.73 x_1 + 5.53) + 1.05 \sin(0.30 x_2 - 1.12) + 1.24 \sin(0.43 x_3 - 7.38) \\
& \left. - 0.54 \sin(6.39 x_4 + 1.00) - 0.06 \sin(0.97 x_5 - 3.63) - 0.86 \sin(0.29 x_6 - 4.05) + 4.07 \right) \\
& + 0.20 \left( 0.34 x_{10} + 0.20 x_{11} + 0.03 x_{13} - 0.08 x_{14} + 0.06 x_{15} + 0.38 x_{17} + 0.06 x_{19} + 0.11 x_{20} \right. \\
& - 0.19 x_{21} + 0.13 x_{22} + 0.09 x_{23} - 0.25 x_{24} + 0.47 x_{25} + 0.23 x_6 + 0.37 x_7 + 0.54 x_8 + 0.04 x_9 \\
& + 0.44 \exp(0.33 x_4) + 0.36 \sin(0.74 x_1 - 6.00) - 0.81 \sin(0.57 x_2 + 8.57) \\
& + 0.75 \sin(0.37 x_3 + 1.79) - 0.63 \sin(0.61 x_5 + 1.78) + 1.99 \left. \right) \\
& \times \left( 0.51 x_{10} + 0.18 x_{11} + 0.18 x_{12} + 0.17 x_{13} - 0.06 x_{14} + 0.06 x_{15} + 0.34 x_{17} + 0.25 x_{20} \right. \\
& - 0.04 x_{21} + 0.19 x_{22} + 0.05 x_{23} - 0.25 x_{24} + 0.46 x_{25} + 0.28 x_6 + 0.38 x_7 + 0.46 x_8 + 0.24 x_9 \\
& - 0.33 \sin(0.91 x_1 - 2.39) - 0.79 \sin(0.63 x_2 + 8.63) + 0.25 \sin(0.63 x_3 + 1.79) \\
& \left. - 0.68 \sin(0.68 x_5 + 8.02) - 0.06 \tan(2.41 x_4 - 9.41) + 2.14 \right) \\
& + 0.05 \sin(0.70 x_1 - 0.31) + 0.41 \sin(0.76 x_1 + 0.40) + 0.21 \sin(1.02 x_1 + 1.37)
\end{aligned}$$

| Dataset | Model       | Metric  | Original | Pruned | Formula | Truncated | causalNN |
|---------|-------------|---------|----------|--------|---------|-----------|----------|
| IHDP-A  | S-KAAM      | MSE     | 1.34     | 2.82   | 2.76    | 2.75      | 1.49     |
|         |             | ATE err | 0.23     | 0.23   | 0.23    | 0.23      | 0.39     |
|         |             | PEHE    | 1.15     | 1.15   | 1.15    | 1.15      | 1.01     |
| ACIC-7  | T-KAAM      | MSE     | 4.84     | 73.77  | 73.93   | 74.21     | 18.80    |
|         |             | ATE err | 0.66     | 2.03   | 2.32    | 2.31      | 0.55     |
|         |             | PEHE    | 5.12     | 5.45   | 7.70    | 7.67      | 7.33     |
| IHDP-B  | Dragon-KAAM | MSE     | 23.82    | 27.87  | 26.79   | 27.40     | 25.94    |
|         |             | ATE err | 0.27     | 0.50   | 0.65    | 0.59      | 0.42     |
|         |             | PEHE    | 2.72     | 2.70   | 4.82    | 4.27      | 2.46     |
| ACIC-2  | Dragon-KAAM | MSE     | 11.20    | 9.69   | 9.45    | 10.53     | 8.32     |
|         |             | ATE err | 0.28     | 2.10   | 2.16    | 2.83      | 0.26     |
|         |             | PEHE    | 2.54     | 2.70   | 2.74    | 3.07      | 1.35     |

Table 2: Pipeline metrics variation across datasets and models. Metrics are rounded to 2 decimals.

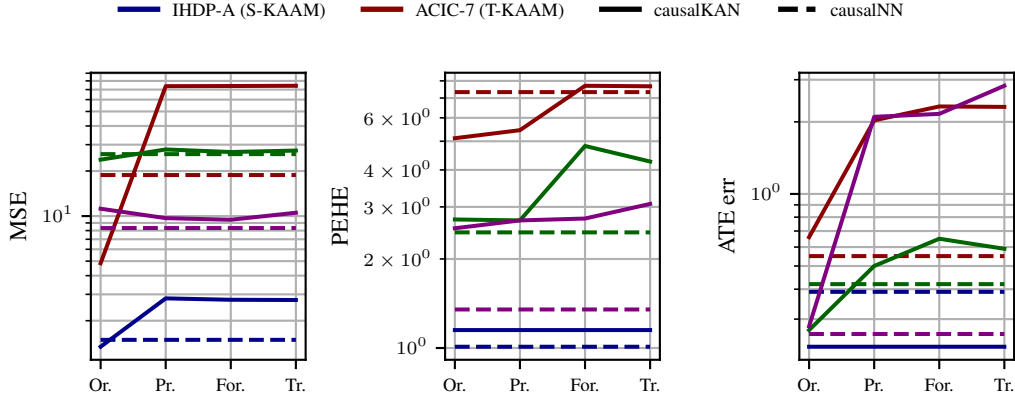


Figure 15: Variation of the metrics in each step of the pipeline: original (Or.), pruned (Pr.), Formula (For.) and 2-decimal truncation (Tr.).

$$\begin{aligned}
& + 0.03 \sin(0.84 x_2 - 6.75) - 0.16 \sin(1.15 x_2 + 2.99) - 0.07 \sin(0.63 x_3 - 3.98) + 1.43 \sin(0.65 x_3 + 2.23) \\
& + 0.33 \sin(0.99 x_3 + 0.79) - 0.16 \sin(6.42 x_4 - 5.19) + 0.68 \sin(6.76 x_4 + 1.83) \\
& - 0.10 \sin(0.69 x_5 - 4.36) - 0.06 \sin(0.70 x_5 + 1.82) + 0.70 \sin(0.75 x_5 - 1.42) \\
& + 0.02 \tan(9.59 x_4 - 8.20) + 0.69 \tanh(0.56 x_5 - 0.36) + 3.79.
\end{aligned}$$

#### C.2.4 METRIC VARIATIONS FOLLOWING THE PIPELINE

We also show how the metrics—both observed (test loss) and unobserved (PEHE) in real data— vary when we perform the pruning and the symbolic substitution in the examples that we develop in §C.2.

We can observe in Fig. 15, for each dataset (with its respective model), the variation in performance when **i)** we prune the network, **ii)** we substitute the splines by symbolic formulas and **iii)** we truncate the formulas to have 2 decimals.

The conclusion of this experiment is that the metric variation in the different steps is high, so a practitioner should be careful when setting the budgets of step acceptance. MSE still shows signs of being a good proxy of the PEHE, representing the variations of the PEHE relatively well.

#### C.3 TIME CONSUMPTION

We are interested in comparing training and inference time of causalKANs with their respective causalNNs. It is well known that KANs take more time to train than MLPs, for networks with the same number of parameters. However, KANs usually require less parameters than MLPs to achieve

similar performance (Liu et al., 2024b). For the tasks analyzed in this paper, causalKANs requires greater computational effort during both training and inference than existing causal neural networks. We consider this additional cost justified by the interpretability that causalKANs provides, which we regard as a central advantage for causal analysis. We report the relative training and inference times in Tab 3.

| Dataset | Model Name | KAN                      |                      | MLP                     |                      | Ratio (Train)<br>KAN/MLP |
|---------|------------|--------------------------|----------------------|-------------------------|----------------------|--------------------------|
|         |            | Training (s)             | Inference (s)        | Training (s)            | Inference (s)        |                          |
| IHDP A  | S-Learner  | 23.62 <sub>19.25</sub>   | 0.12 <sub>0.02</sub> | 1.98 <sub>2.05</sub>    | 0.00 <sub>0.00</sub> | 12                       |
|         | T-Learner  | 97.89 <sub>75.57</sub>   | 0.03 <sub>0.01</sub> | 29.00 <sub>29.19</sub>  | 0.00 <sub>0.00</sub> | 7/2                      |
|         | TarNet     | 67.21 <sub>52.39</sub>   | 0.01 <sub>0.00</sub> | 8.02 <sub>9.27</sub>    | 0.00 <sub>0.00</sub> | 8/1                      |
|         | DragonNet  | 62.92 <sub>48.39</sub>   | 0.01 <sub>0.00</sub> | 9.74 <sub>10.28</sub>   | 0.00 <sub>0.00</sub> | 6/1                      |
| IHDP B  | S-Learner  | 56.24 <sub>22.13</sub>   | 0.06 <sub>0.01</sub> | 2.61 <sub>1.24</sub>    | 0.00 <sub>0.00</sub> | 22                       |
|         | T-Learner  | 58.49 <sub>14.10</sub>   | 0.03 <sub>0.00</sub> | 45.81 <sub>18.08</sub>  | 0.00 <sub>0.00</sub> | 9/7                      |
|         | TarNet     | 31.39 <sub>10.88</sub>   | 0.03 <sub>0.00</sub> | 42.37 <sub>16.43</sub>  | 0.00 <sub>0.00</sub> | 3/4                      |
|         | DragonNet  | 157.82 <sub>38.35</sub>  | 0.01 <sub>0.00</sub> | 187.26 <sub>31.89</sub> | 0.00 <sub>0.00</sub> | 5/6                      |
| ACIC 2  | S-Learner  | 120.96 <sub>54.54</sub>  | 0.05 <sub>0.01</sub> | 23.13 <sub>15.77</sub>  | 0.00 <sub>0.00</sub> | 5/1                      |
|         | T-Learner  | 368.94 <sub>153.74</sub> | 0.22 <sub>0.03</sub> | 162.59 <sub>28.60</sub> | 0.01 <sub>0.00</sub> | 9/4                      |
|         | TarNet     | 135.38 <sub>83.87</sub>  | 0.05 <sub>0.01</sub> | 55.08 <sub>62.84</sub>  | 0.01 <sub>0.00</sub> | 5/2                      |
|         | DragonNet  | 92.83 <sub>55.77</sub>   | 0.04 <sub>0.01</sub> | 63.17 <sub>70.06</sub>  | 0.01 <sub>0.00</sub> | 3/2                      |
| ACIC 7  | S-Learner  | 147.31 <sub>110.57</sub> | 0.23 <sub>0.03</sub> | 4.56 <sub>7.80</sub>    | 0.00 <sub>0.00</sub> | 32                       |
|         | T-Learner  | 377.66 <sub>177.18</sub> | 0.04 <sub>0.01</sub> | 39.90 <sub>43.24</sub>  | 0.01 <sub>0.00</sub> | 9/1                      |
|         | TarNet     | 236.88 <sub>109.75</sub> | 0.03 <sub>0.00</sub> | 40.38 <sub>50.22</sub>  | 0.01 <sub>0.00</sub> | 6/1                      |
|         | DragonNet  | 272.19 <sub>127.14</sub> | 0.03 <sub>0.00</sub> | 51.86 <sub>65.79</sub>  | 0.01 <sub>0.00</sub> | 5/1                      |
| ACIC 26 | S-Learner  | 141.11 <sub>96.81</sub>  | 0.17 <sub>0.02</sub> | 4.46 <sub>7.54</sub>    | 0.00 <sub>0.00</sub> | 32                       |
|         | T-Learner  | 145.50 <sub>70.85</sub>  | 0.03 <sub>0.00</sub> | 39.36 <sub>42.07</sub>  | 0.01 <sub>0.00</sub> | 7/2                      |
|         | TarNet     | 111.13 <sub>53.19</sub>  | 0.02 <sub>0.00</sub> | 39.89 <sub>49.73</sub>  | 0.01 <sub>0.00</sub> | 8/3                      |
|         | DragonNet  | 147.49 <sub>70.45</sub>  | 0.03 <sub>0.05</sub> | 48.26 <sub>58.27</sub>  | 0.01 <sub>0.00</sub> | 3/1                      |

Table 3: Comparison of training and inference times (in seconds) for KAN and MLP across datasets. The last column shows the ratio of KAN to MLP training time, approximated as simple fractions. Values are reported as mean<sub>std</sub>.

In average, causalKANs train slower than causalNNs: KAN training time  $\approx 8 \times$  MLP training time.

#### C.4 COMPARISON VISUALIZATIONS

In the same fashion, we have compared each causalNN with its respective causalKAN , in Fig. 16.

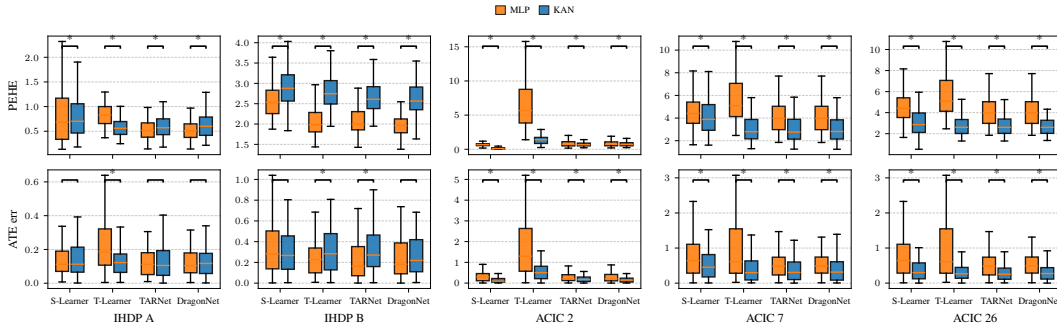


Figure 16: Comparison of KAN vs MLP across datasets. Top row: PEHE, bottom row: ATE err. The trend of the difference is not constant across datasets. For example, we can observe that causalKANs achieve better PEHE metrics in IHDP A and ACIC 2/7/26, but worse in IHDP B, than their respective causalNNs.

We also include, in Tab 4, p-values for transparency, as they provide a more nuanced understanding of the evidence against the null hypothesis than a binary significant/non-significant determination at a fixed  $\alpha$  level.

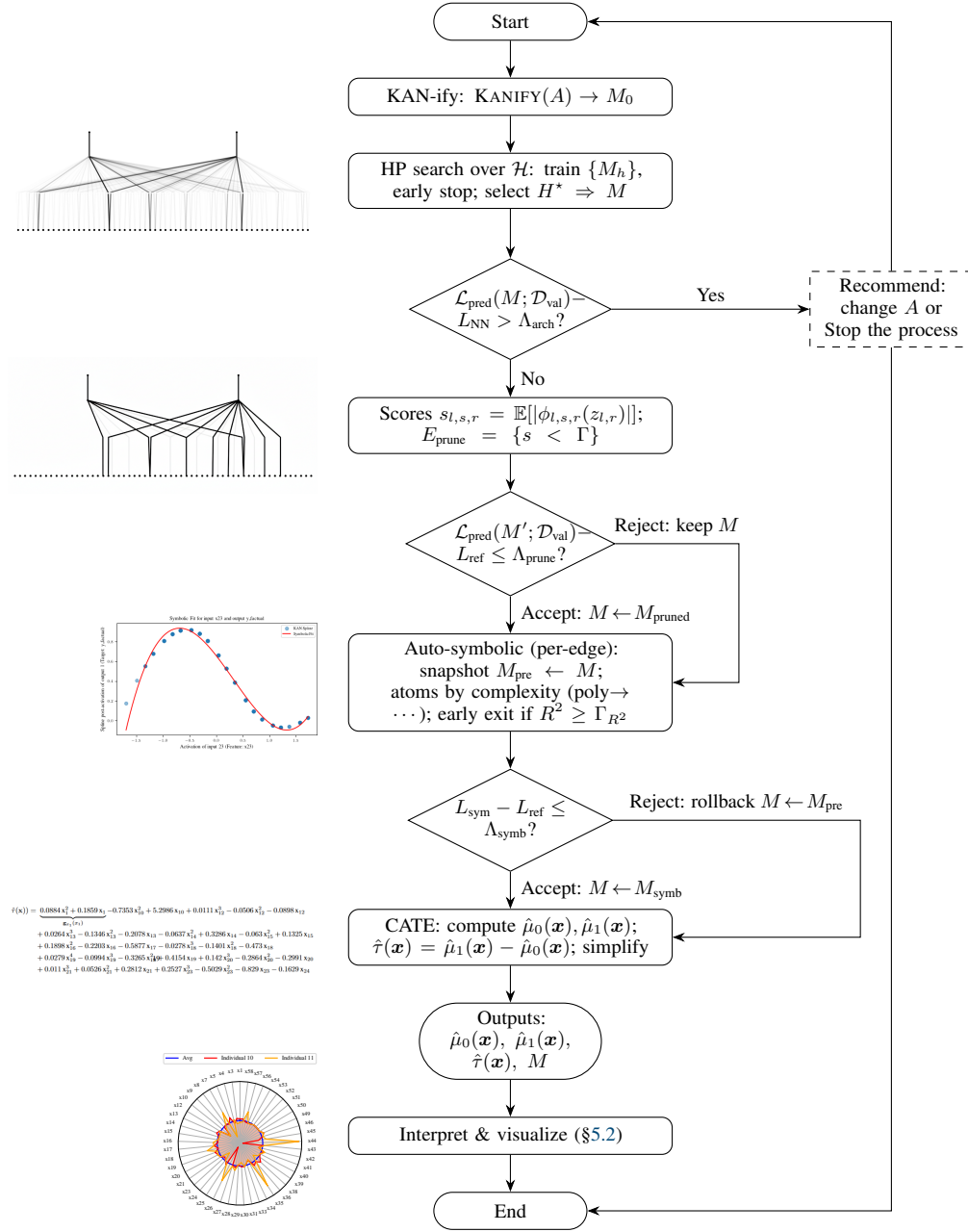
| Dataset | Architecture | KAN           |              | MLP           |              |
|---------|--------------|---------------|--------------|---------------|--------------|
|         |              | $p$ (ATE err) | $p$ (PEHE)   | $p$ (ATE err) | $p$ (PEHE)   |
| IHDP A  | S-Learner    | <b>0.781</b>  | <b>0.121</b> | <b>0.132</b>  | $< 10^{-3}$  |
|         | T-Learner    | <b>0.889</b>  | <b>1.000</b> | $< 10^{-3}$   | $< 10^{-3}$  |
|         | TarNet       | <u>1.000</u>  | <b>1.000</b> | <b>0.906</b>  | <b>1.000</b> |
|         | DragonNet    | <b>0.906</b>  | <b>1.000</b> | <b>1.000</b>  | <b>1.000</b> |
| IHDP B  | S-Learner    | 0.006         | $< 10^{-3}$  | 0.012         | $< 10^{-3}$  |
|         | T-Learner    | 0.007         | $< 10^{-3}$  | <b>0.388</b>  | <b>0.189</b> |
|         | TarNet       | 0.003         | $< 10^{-3}$  | <b>1.000</b>  | <b>0.189</b> |
|         | DragonNet    | <b>0.388</b>  | <b>0.006</b> | <b>0.436</b>  | <b>1.000</b> |
| ACIC 2  | S-Learner    | <b>1.000</b>  | <b>1.000</b> | $< 10^{-3}$   | $< 10^{-3}$  |
|         | T-Learner    | $< 10^{-3}$   | $< 10^{-3}$  | $< 10^{-3}$   | $< 10^{-3}$  |
|         | TarNet       | 0.013         | $< 10^{-3}$  | $< 10^{-3}$   | $< 10^{-3}$  |
|         | DragonNet    | <b>0.157</b>  | $< 10^{-3}$  | $< 10^{-3}$   | $< 10^{-3}$  |
| ACIC 7  | S-Learner    | 0.020         | $< 10^{-3}$  | $< 10^{-3}$   | $< 10^{-3}$  |
|         | T-Learner    | <b>0.908</b>  | <b>0.788</b> | $< 10^{-3}$   | $< 10^{-3}$  |
|         | TarNet       | <b>1.000</b>  | <b>0.788</b> | 0.020         | $< 10^{-3}$  |
|         | DragonNet    | <b>0.706</b>  | <b>1.000</b> | $< 10^{-3}$   | $< 10^{-3}$  |
| ACIC 26 | S-Learner    | <b>0.838</b>  | 0.022        | $< 10^{-3}$   | $< 10^{-3}$  |
|         | T-Learner    | <b>1.000</b>  | <b>0.511</b> | $< 10^{-3}$   | $< 10^{-3}$  |
|         | TarNet       | <b>1.000</b>  | <b>0.511</b> | 0.011         | $< 10^{-3}$  |
|         | DragonNet    | <b>1.000</b>  | <b>1.000</b> | $< 10^{-3}$   | $< 10^{-3}$  |

Table 4: Friedman post-hoc *corrected*  $p$ -values per dataset and metric, arranged to mirror [Tab 1](#). Baselines are underlined (reported as  $p = 1.000$ ) and methods not significantly different from the baseline at  $\alpha = 0.05$  are in **bold**. Very small  $p$ -values are reported as  $< 10^{-3}$ .

## D COMPLETE PIPELINE

We offer two different complete visualizations of the pipeline that we propose, in an algorithm [Alg. 1](#) version that details all the steps, including the details and the computational step of each block, and a block diagram [Fig. 17](#) in which is easier to focus on the decision steps and the importance of the budgets.

As can be observed, although the pipeline is well defined, there are many variables (or hyperparameters) that the practitioner should vary depending on the dataset or the application of our proposal.



**Legend:**  $\Gamma$  pruning threshold;  $\Gamma_{R^2}$  per-edge symbolic  $R^2$  threshold;  $\Lambda_{\text{arch}}$  KAN vs NN loss budget;  $\Lambda_{\text{prune}}$  pruning budget;  $\Lambda_{\text{symb}}$  global symbolic budget;  $L_{\text{ref}}$  current best validation loss;  $L_{\text{sym}}$  validation loss after symbolification.

Figure 17: Block diagram of CausalKAN pipeline with explicit Accept/Reject semantics and final outputs.



---

**Algorithm 1** CausalKAN : Interpretable CATE via KAN-ified causal networks

---

**Input:** Base causalNN  $A$ ; splits  $\mathcal{D}_{\text{tr}}, \mathcal{D}_{\text{val}}, \mathcal{D}_{\text{te}}$  with  $(\mathbf{x}, \mathbf{t}, \mathbf{y})$ ; budgets  $\Lambda_{\text{prune}}, \Lambda_{\text{symb}}$ ; thresholds  $\Gamma$  (prune),  $\Gamma_{R^2}$  (symbolic),  $\Lambda_{\text{arch}}$  (KAN vs NN); HP spaces,  $\mathcal{H}$ , (depth, width, spline grid,  $\lambda_1, \lambda_c, \lambda_s, \lambda_H$ ); atom dict  $\{f_m\}_{m=1}^M$  ordered by complexity (poly  $\rightarrow$  trigs  $\rightarrow$  others); optimizer, early stopping.

**Output:**  $\hat{\mu}_0(\mathbf{x}), \hat{\mu}_1(\mathbf{x}), \hat{\tau}(\mathbf{x}) \equiv \hat{\mu}_1(\mathbf{x}) - \hat{\mu}_0(\mathbf{x})$

```

1: KAN-ification:  $M_0 \leftarrow \text{KANIFY}(A)$ 

2: HP search & training:
3: for  $h \in \mathcal{H}$  do
4:    $M_h \leftarrow \text{INSTANTIATE}(M_0, h)$ 
5:   Minimize on  $\mathcal{D}_{\text{tr}}$ :

$$\mathcal{L} = \mathcal{L}_{\text{pred}}(M_h) + \lambda_1 \sum_{l,s,r} \mathbb{E}[|\phi_{l,s,r}(z_{l,r})|] + \lambda_c \sum |w_s| + \lambda_s \sum |w_s - w'_s| + \lambda_H \sum H$$


6:   Early stop on  $\mathcal{D}_{\text{val}}$ ; store  $L_{\text{val}}(h) = \mathcal{L}_{\text{pred}}(M_h^\dagger; \mathcal{D}_{\text{val}})$ 
7: end for
8:  $H^* \leftarrow \arg \min_h L_{\text{val}}(h)$  with tie-break by simplicity (fewer layers, smaller grids/nodes, no MultKAN)
9:  $M \leftarrow M_{H^*}^\dagger$ ;  $L_{\text{ref}} \leftarrow L_{\text{val}}(H^*)$ 

10: Baseline causalNN check (KAN vs NN):
11: Train  $A^\dagger$  (original causalNN) under its best HPs on  $\mathcal{D}_{\text{tr}}$  with early stopping
12:  $L_{\text{NN}} \leftarrow \mathcal{L}_{\text{pred}}(A^\dagger; \mathcal{D}_{\text{val}})$ 
13: if  $\mathcal{L}_{\text{pred}}(M; \mathcal{D}_{\text{val}}) - L_{\text{NN}} > \Lambda_{\text{arch}}$  then
14:   Warn/Recommend: change  $A$  (architecture underperforming);
15: end if

16: Pruning (accept-reject):
17:  $s_{l,s,r} \leftarrow \mathbb{E}_{\mathcal{D}_{\text{val}}} [|\phi_{l,s,r}(z_{l,r})|]$ 
18:  $E_{\text{prune}} \leftarrow \{(l, s \rightarrow r) : s_{l,s,r} < \Gamma\}$ 
19: if  $E_{\text{prune}} \neq \emptyset$  then
20:    $M' \leftarrow \text{REMOVEEDGESANDISOLATEDNODES}(M, E_{\text{prune}})$ 
21:   if  $\mathcal{L}_{\text{pred}}(M'; \mathcal{D}_{\text{val}}) - L_{\text{ref}} \leq \Lambda_{\text{prune}}$  then
22:      $M \leftarrow M'$ ;  $L_{\text{ref}} \leftarrow \mathcal{L}_{\text{pred}}(M; \mathcal{D}_{\text{val}})$ 
23:   else
24:     Reject pruning
25:   end if
26: end if

27: Auto-symbolic (per-edge, early exit by  $R^2$ ) + global accept:
28:  $M_{\text{pre}} \leftarrow M$  ▷ snapshot for possible rollback
29: for each edge  $e = (l, s \rightarrow r)$  in  $M$  do
30:   collect  $\{(u_k, v_k)\}$  on  $\mathcal{D}_{\text{val}}$ :  $u_k = z_{l,r}^{(k)}, v_k = \phi_{l,s,r}(u_k)$ 
31:   for  $m = 1 \rightarrow M$  (complexity-ordered) do
32:      $(a^*, b^*, c^*, d^*) \leftarrow \arg \min_{a,b,c,d} \frac{1}{|\mathcal{D}_{\text{val}}|} \sum_k (v_k - [cf_m(au_k + b) + d])^2$ 
33:     compute  $R_m^2$  on  $\mathcal{D}_{\text{val}}$ 
34:     if  $R_m^2 \geq \Gamma_{R^2}$  then
35:        $M \leftarrow \text{REPLACEEDGEWITHATOM}(M, e, f_m, a^*, b^*, c^*, d^*)$  ▷ early accept for this edge
36:       break
37:     end if
38:   end for
39: end for
40:  $L_{\text{sym}} \leftarrow \mathcal{L}_{\text{pred}}(M; \mathcal{D}_{\text{val}})$ 
41: if  $L_{\text{sym}} - L_{\text{ref}} \leq \Lambda_{\text{symb}}$  then
42:   Accept symbolic model;  $L_{\text{ref}} \leftarrow L_{\text{sym}}$ 
43: else
44:   Reject symbolic model;  $M \leftarrow M_{\text{pre}}$ 
45: end if

46: CATE extraction (difference  $\Rightarrow$  simplify):
47: Compute  $\hat{\mu}_0(\mathbf{x}), \hat{\mu}_1(\mathbf{x})$  by forward evaluation of the two heads
48:  $\hat{\tau}(\mathbf{x}) \leftarrow \hat{\mu}_1(\mathbf{x}) - \hat{\mu}_0(\mathbf{x})$ 
49:  $\text{SIMPLIFYALGEBRA}(\hat{\tau}(\mathbf{x}))$  ▷ cancel/factor common terms after the difference
50: return  $(\hat{\mu}_0, \hat{\mu}_1, \hat{\tau}(\mathbf{x}), M)$ 

```

---